

ABSTRACT

EFFECTS OF CONFINING PRESSURE ON POLYCRYSTALLINE ROCK BEHAVIOR ANALYSED BY RHEOLOGICAL THEORY

by Ezra D. Shoua

The influence of confining pressure upon stress distribution and deformation fields of polycrystalline rock under load has heretofore been studied theoretically through empirical relations which have serious shortcomings in describing accurately characteristic rock behavior. This inadequacy may be attributed in part to the fact that rock is a heterogeneous material whose crystals possess physical properties which differ from the grain boundary properties.

In this investigation, the rock behavior is simulated by a rheological model composed of two independent systems, one representing the crystal properties and the second the properties of the grain boundaries. This unique arrangement offers a means whereby in the mathematical analysis the separate contributions of the crystals and grain boundaries are correlated to the degree of confinement. This rheological description of rock behavior not only yields results in good agreement with existing experimental data but furthermore provides a basis for understanding the variation of physical constants with changes in confining pressure.

EFFECTS OF CONFINING PRESSURE ON POLYCRYSTALLINE
ROCK BEHAVIOR ANALYSED BY RHEOLOGICAL
THEORY

By

Ezra David Shoua

A THESIS

Submitted to
Michigan State University
in partial fulfillment of the requirements
for the degree of

DOCTOR OF PHILOSOPHY

Department of Civil Engineering

1965



ACKNOWLEDGMENTS

The author would like to express his deep gratitude for the guidance of Dr. George E. Mase, Professor of Applied Mechanics and acting Chairman, of the Metallurgy, Mechanics and Material Science Department, under whose supervision this study was conducted.

Special thanks are due to Dr. L. E. Malvern, Professor of Applied Mechanics, for his valuable suggestions during the formulation of this analysis; to Dr. O. B. Andersland, Associate Professor of Civil Engineering, for his interest and help whenever requested, to Dr. J. L. Lubkin, Professor of Civil Engineering and Applied Mechanics for serving on his committee, and to Dr. S. Serata, Associate Professor of Civil Engineering for introducing the writer to the field of rock mechanics.

Thanks go to the National Science Foundation and to the Division of Engineering Research at Michigan State University for the financial assistance rendered during part of the writer's doctoral program.

TABLE OF CONTENTS

ACKNOWLEDGMENTS	ii
LIST OF TABLES	v
LIST OF FIGURES	vi
NOTATION	ix
 Chapter	 Page
I. INTRODUCTION	1
1.1 Statement of the problem	1
1.2 Literature survey	2
1.3 Scope and objectives	6
II. ANALYSIS OF MATERIAL CHARACTERISTICS	8
2.1 Structure of the material	8
2.2 Definition and elastic relationships between differential stress and differential strain	9
2.3 Possible criteria of testing	11
2.4 Behavior of material under different testing conditions	15
III. THEORETICAL ANALYSIS	20
3.1 Proposed rheological model	20
3.2 Assumptions	25
3.3 Variation of behavior with confining pressure	26
3.3a Variation of the equivalent elastic response with the degree of confinement	31
3.3b Variation of the equivalent visco- elastic response with the degree of confinement	32
3.3c Variation of the equivalent visco- plastic response with the degree of confinement	41
IV. APPLICATION AND PREDICTIONS OF THEORY	45
4.1 Variation of the elastic modulus E_{eq} with confining pressure	45

TABLE OF CONTENTS - Continued

Chapter	Page
4.2 Variation of the visco-elastic range with confining pressure	51
4.3 Variation of the visco-plastic dif- ferential strain rate with confining pressure	58
V. SUMMARY AND CONCLUSIONS	60
5.1 Discussion	60
5.2 Future research	63
BIBLIOGRAPHY	65

LIST OF TABLES

Table	Page
3.1 Calculations of E_{eq} vs c for different values of α	33

LIST OF FIGURES

Figure	Page
1.1 Schematic diagram of Adams' apparatus for testing rocks under high confining pressure (after Adams and Bancroft) ³	2
1.2 Griggs' early apparatus (after Griggs) ¹⁵	4
1.3 Griggs' later apparatus (after Griggs) ¹⁷	5
2.1 Polycrystalline rock salt specimen showing randomly oriented crystals	8
2.2 General triaxial principal stress state	9
2.3 Hydrostatic confining stress state	10
2.4 Differential stress state	10
2.5 Uniaxial differential stress state	12
2.6 Balanced biaxial differential stress state	13
2.7 General biaxial differential stress state	14
2.8 Variation of E_{eq} with m	15
2.9 Idealized stress-strain diagram	16
2.10 Failure of rock salt specimen tested under uniaxial differential stress with a confining pressure equal to one atmosphere	17
2.11 Failure of rock salt specimen tested under a balanced biaxial differential stress with a confining pressure equal to one atmosphere	17
2.12 Failure of rock salt specimen tested under uniaxial differential stress with a confining pressure equal to one hundred atmospheres	18
3.1 Graph representing the different creep curves at varying magnitudes of differential stress	20
3.2 Typical creep curve at constant differential stress	21

Figure	Page
3.3 Burgers model showing the relationship between differential strain rate and differential stress for the steady-state or visco-plastic creep	24
3.4 SVB model showing the relationship between differential strain rate and differential stress for the steady-state or visco-plastic creep	24
3.5 Proposed mechanical model	25
3.6 Differential stress-strain-time relationship . . .	27
(a) Deformation of model due to applied differential stress	27
(b) History of loading	27
3.7 Typical variation of E_{eq} with c	32
3.8 Variation of E_{eq} vs. c for various values of α . .	34
3.9 Variation of the visco-elastic creep with time . .	37
3.10 Variation of the range with the degree of confinement	37
3.11 Variation of visco-elastic creep with the degree of confinement for case (a)	39
3.12 Variation of visco-elastic creep with the degree of confinement for case (b)	40
3.13 Relationship between differential strain rate and differential stress for the steady state response	43
3.14 Relationship between differential strain rate and degree of confinement	44
4.1 Differential stress-strain curves of rock salt specimens deformed in compression (after J. Handin (1953) ¹⁸)	46
4.2 Graph of E_{eq} vs. p for rock salt at constant room temperature	48
4.3 Differential stress-strain curves for Solenhofen limestone (after H. C. Heard) ²⁰	49
4.4 Graph of E_{eq} vs. p for Solenhofen Limestone at a constant room temperature of 25° C.	50

Figure	Page
4.5 Creep test results on Solenhofen Limestone specimens (after E. C. Robertson ²⁸)	52
4.6 Creep test results on Solenhofen Limestone (after Robertson (1960) ²⁸)	53
4.7 Normalized visco-elastic creep curves of Solenhofen Limestone at different confining pressures and same differential stress	55
4.8 Comparison of the effect of confining pressure on the range and initial slope of the visco-elastic curves of Solenhofen Limestone	56
4.9 Comparison of theoretical and actual test results for the variation of the range with confining pressure at constant differential stress ($S=1500 \text{ kg/cm}^2$)	57

NOTATION

α	principal compressive stress
ϵ'	principal strain
ϵ''	strain caused by hydrostatic confining stress
ϵ	differential strain
μ	poisson's ratio
m	ratio of ϵ_y to ϵ_x
S	differential stress
E_{eq}	equivalent elastic modulus
E_1, E_1^*	elastic constants of grain boundary bonds
η_1^*	visco-elastic coefficient of boundary bonds
η_1	visco-plastic coefficient of boundary bonds
Y_1	differential yield strength of boundary bonds
E_2, E_2^*	elastic constants of crystal grains
η_2	visco-elastic coefficient of crystal grains
η_2^*	visco-plastic coefficient of crystal grains
Y_2	differential yield strength of crystal grains
t	time
c	degree of confinement
p	confining pressure
α	ratio of E_2 to E_1
α^*	Ratio of E_2^* to E_1^*
τ_1	Ratio of E_1^* to μ_1^*
τ_2	Ratio of E_2^* to η_2^*

β^*	ratio of $1/\tau_2$ to $1/\tau_1$
β	ratio of η_2 to η_1
λ	ratio of Y_2 to Y_1
R	range of visco-elastic creep
G	hydrostatic elastic constant

CHAPTER I

INTRODUCTION

1.1 Statement of the Problem

Geologists have long recognized that while most rocks are capable of sustaining a rather large amount of flow with little accompanying fracture in highly contorted regions of the earth's crust, these same rocks exhibit an exceedingly brittle behavior when deformed under ordinary atmospheric conditions.

This great increase in ductility within the earth's crust has been attributed to the environmental conditions thought to have existed at the time of deformation, and is ascribed to the effect of any combination of the following five significant factors:

1. Confining compressive pressure
2. Differential compressive pressure
3. Duration of time
4. High temperatures
5. Presence of solutions

Although these facts have been known for many years, only since the turn of the century have investigators begun to study the mechanical properties of rocks by attempting to simulate in the laboratory the complex conditions under which

they exist in underground formations.

1.2 Literature Survey

This transition from brittle fracture to ductile flow in triaxially confined tested rock samples was first qualitatively shown to be dependent upon confining pressure by Adams and Nicolson (1901)¹ and later by Adams (1910)² and (1912)³ and by Adams and Bancroft (1917)⁴ when they compressed small cylinders of marble specimens under a con-

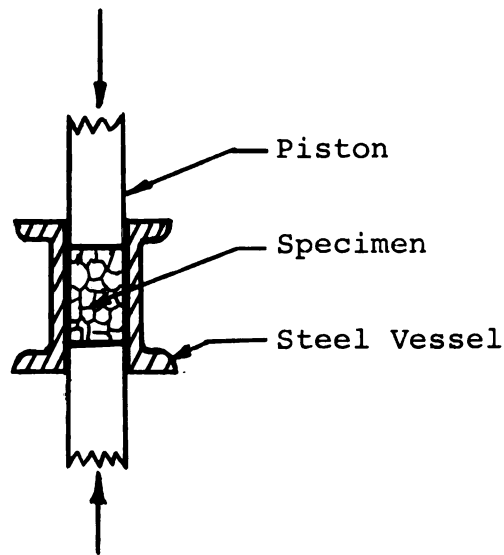


Fig. 1.1 Schematic Diagram of Adams' Apparatus for Testing Rocks Under High Confining Pressure (After Adams and Bancroft)³

fining pressure provided by the walls of a steel vessel.

Their technique, however, had the following disadvantages:

- (i) The confining pressure varied during the experiment.
- (ii) The confining pressure could not be accurately computed because of friction between a rock specimen and the steel vessel.
- (iii) The specimen was not free to fracture.

These findings were later verified quantitatively by Von Karman (1911)³³ and his student Böker (1915)⁷. They obtained accurate stress-strain diagrams by deforming jacketed cylindrical specimens of Carrara marble and red sandstone in an apparatus which permitted compressive loading of samples subjected externally to liquid pressures of several thousand atmospheres. Their results indicated that marble under high confining pressure behaved much like a ductile material capable of sustaining large permanent deformations.

In 1936 Griggs¹⁵ published a series of important contributions to the problem of rock deformation utilizing more precise equipment. His early apparatus (as shown diagrammatically in Fig. 1.2) was designed for use up to a maximum pressure of 13,000 atmospheres, or the equivalent of about 28 miles deep in the earth's crust.

Among the significant results of his work on marble and limestone are the increase in the elastic limit and the ultimate strength with increase in confining pressure and their dependence upon the duration of the test.

More improved techniques and testing apparatus capable of handling up to 50,000 atmospheres of pressure were later used by Griggs (1939)¹⁶ (1940)¹⁷ to study the effects of time, temperature and the chemical environment of solutions.

One of the important outcomes of his study was the presentation of an empirical equation which describes the creep of rock in compression in which he suggests that the total strain $\epsilon(t)$ at any time t can be represented by the relationship

$$\epsilon(t) = A + B \log t + C t \quad (1.2-1)$$

in which A, B, and C are constants of the material.

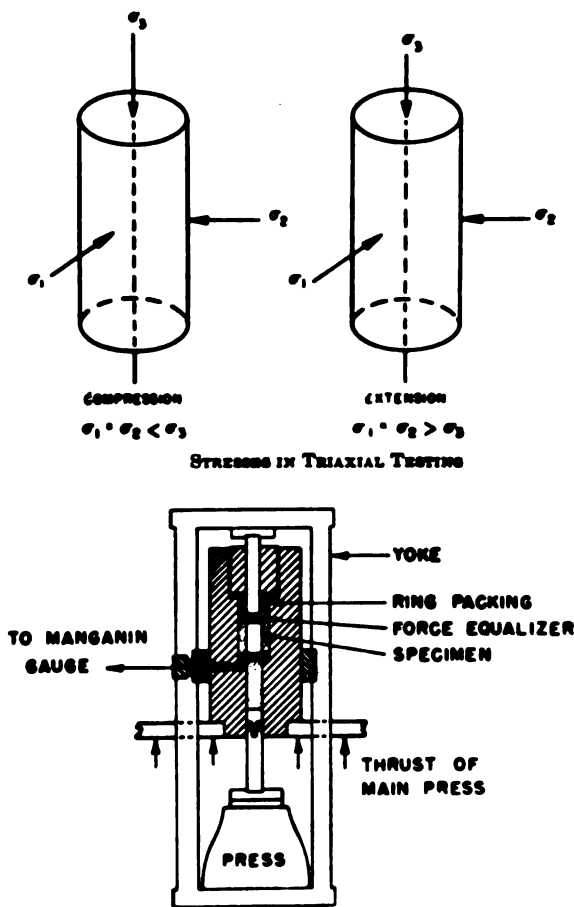


Fig. 1.2 Griggs' Early Apparatus (After Griggs)¹⁵

More organized and systematic tests displaying the effect of confining pressure were then performed by a number of Geophysical research workers. Among them is Handin's work (1953)¹⁸ in which he obtained stress-strain curves of rock salt deformed in compression, and Handin and Hager (1957)¹⁹ in which stress-strain curves for a variety of polycrystalline rocks were presented. More recently, tests were performed by Heard (1960)²⁰ in which stress-strain curves of Solenhofen Limestone specimens (confined up to 5,000 atmospheres) were obtained at different constant temperatures.

In addition, tests were performed to evaluate the interstitial fluid pressure effect within the interstices of a rock subjected to high confining pressures during a triaxial test.

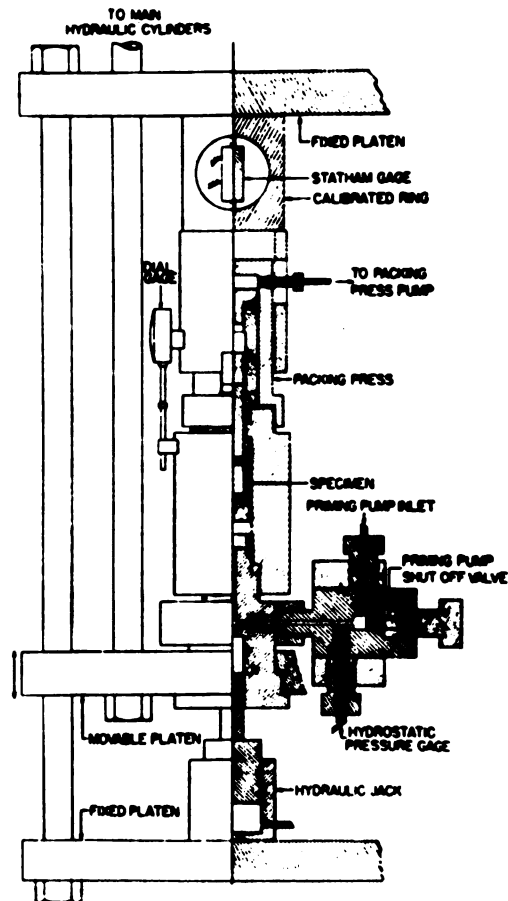


Fig. 1.3 Griggs' Later Apparatus (After Griggs)¹⁷

Brace (1963)⁸ tested the ultimate strength of rocks both in tension and compression, while Baron et al (1963)⁵ attempted to analyse both the dynamic and static elastic constants for several types of rocks at various degrees of confinement. In all of these studies data was compiled together with analytic observation of microscopic fabric changes in an attempt to establish the deformation mechanism that is involved.

Although elastic and fracture properties were thoroughly investigated, very little systematic tests were done on the creep behavior of polycrystalline rocks. Robertson (1960)²⁸ carried the second and only organized creep testings on Solenhofen Limestone specimens at constant room temperatures and different confining pressures that varied up to 4,000 bars. Some of his important conclusions were:

1. The creep behavior of polycrystalline rocks exhibit three distinct stages: transient, steady state and accelerating.
2. The following empirical relationship was deduced

$$t\epsilon = K_1 = K_2S - K_3 \quad (1.2-2)$$

which fits the time t , transient creep strain rate ϵ and differential stress S of the experiments; K_1 , K_2 , and K_3 being constants for a given confining pressure p .

1.3 Scope and Objectives

Geologists and Geomechanic investigators have long known that the behavior of polycrystalline rocks under load are influenced by the five factors mentioned previously in Sec. 1.1, but they have been unable to establish a satisfactory theory correlating any combination of these factors so that such a characteristic behavior could be explained or predicted.

The first attempt by Griggs (1939)¹⁷, Robertson (1960)²⁸ and others was to establish empirical relationships in an effort to explain some aspects of such a behavior. However,

it was found that the empirical relations could neither fit the whole range of all the results obtained nor account for the actual mechanism of the stress-strain-time relationship.

More recently, inspired by the application of mechanical models to simulate viscoelastic creep behavior, several efforts were made by Emery (1963)¹², Price (1964)²⁶, and others to establish a satisfactory model that would represent the characteristic mechanism of polycrystalline rock. These mechanical models mostly simulated uniaxial behavior only and failed to explain the transitional behavior from the uniaxial to the triaxial state of stress.

In this presentation, based on observation of the research work done so far on these polycrystalline rocks, a new mechanical model is proposed in which differential strain and time are related as a function of both the differential stress and the confining pressure, which accounts for the change in behavior that is displayed over the range between the uniaxial and triaxial stress states.

In view of the above, possible testing criteria are established, thus demonstrating a need for the additional systematic experiments which are proposed.

CHAPTER II

ANALYSIS OF MATERIAL CHARACTERISTICS

2.1 Structure of the Material

Polycrystalline rocks exist as a compact composition of an aggregate of crystal grains having various shapes and orientations. Theory and experiment suggest that between a crystal grain of one orientation and other neighboring ones, there exists a grain boundary layer only a few atoms thick in which randomly arranged atoms take up equilibrium positions

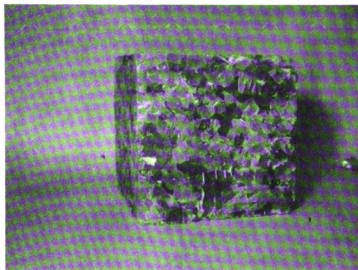


Fig. 2.1 Polycrystalline Rock Salt Specimen Showing Randomly Oriented Crystals

and possess a higher free energy than the compact geometrical arrangement of the atoms within the crystal grains.

The mechanical properties of such a single-phase aggregate are determined mainly by two factors:

- (a) the properties of the crystals of the aggregate, and
- (b) the properties of the amorphous grain boundary which binds these individual crystals together to form the composite mass.

2.2 Definition and Elastic Relationships Between Differential Stress and Differential Strain

In order to simulate the behavior of the above polycrystalline material under load, it is important to define the stress state that governs its deformation.

Consider a general state of triaxial principal stress condition with σ_x , σ_y , and σ_z acting in the x, y, z directions respectively, with $\sigma_x > \sigma_y > \sigma_z$. (For simplicity σ_z will always be considered as the smallest principal stress.) Compressive stress is considered positive.

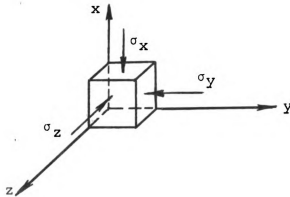


Fig. 2.2 General Triaxial Principal Stress State

This general state of triaxial stress is equivalent to a hydrostatic confining stress tensor, σ_z , acting in the x, y, z directions, plus a differential stress state tensor, S_i , defined as

$$S_i = (\sigma_i - \sigma_z) \quad (2.2-1)$$

acting in the x, y directions only.

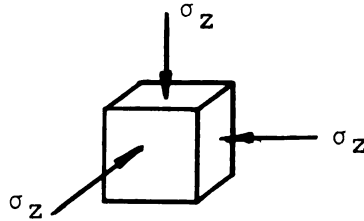


Fig. 2.3 Hydrostatic Confining Stress State

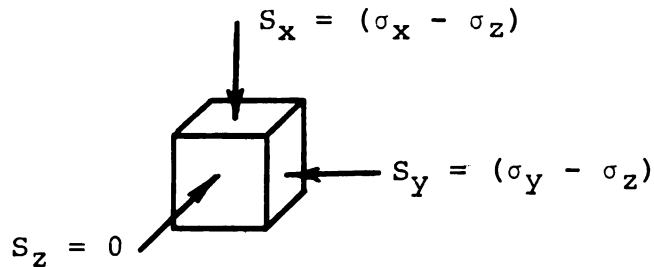


Fig. 2.4 Differential Stress State

Corresponding to the above defined stress conditions, the state of triaxial elastic strain is given by

$$\begin{aligned} E\varepsilon'_x &= \sigma_x - \mu(\sigma_y + \sigma_z) && \text{in the x-direction} \\ E\varepsilon'_y &= \sigma_y - \mu(\sigma_x + \sigma_z) && \text{in the y-direction} \\ E\varepsilon'_z &= \sigma_z - \mu(\sigma_x + \sigma_y) && \text{in the z-direction} \end{aligned} \quad (2.2-2)$$

which can be resolved into a strain, ϵ_i'' caused by the hydrostatic confining stress, namely

$$E\epsilon_i'' = \sigma_z - \mu(\sigma_z + \sigma_z) \quad \text{in the x, y, z-directions (2.2-3)}$$

and a strain caused by the differential stress tensor, defined as differential strain tensor, ϵ_i which is given by

$$E\epsilon_x = E(\epsilon'_x - \epsilon''_x) = (\sigma_x - \sigma_z) - \mu[(\sigma_y - \sigma_z) + (\sigma_z - \sigma_z)]$$

or $E\epsilon_x = S_x - \mu S_y$ in the x-direction

$$E\epsilon_y = S_y - \mu S_x \quad \text{in the y-direction (2.2-3)}$$

$$E\epsilon_z = -\mu(S_x + S_y) \quad \text{in the z-direction}$$

from which

$$\frac{\epsilon_z}{\epsilon_x + \epsilon_y} = \frac{-\mu}{1 - \mu} \quad (2.2-5)$$

if we define

$$m = \frac{\epsilon_y}{\epsilon_x} \quad (2.2-6)$$

then we get the relationship

$$\frac{\epsilon_z}{\epsilon_x} = \frac{-(1 + m)\mu}{1 - \mu} \quad (2.2-7)$$

2.3 Possible Criteria of Testing

With the above definitions, there are three possible cases of loading: (i) uniaxial differential stress state, (ii) balanced biaxial differential stress state, and, (iii) general biaxial differential stress state. Cases (i) and (ii) represent the extreme conditions; the general testing pattern is represented by case (iii).

Case (i) Uniaxial Differential Stress State

in which

$$\sigma_x > \sigma_y = \sigma_z \geq 0$$

giving

$$\left[\begin{array}{ccc} S_x = (\sigma_x - \sigma_z) & - & - \\ - & S_y = 0 & - \\ - & - & S_z = 0 \end{array} \right] \quad (2.3-1)$$

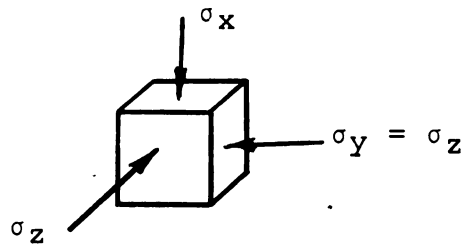


Fig. 2.5 Uniaxial Differential Stress State

and $E\epsilon_x = S_x$

$$E\epsilon_y = -\mu S_x \quad (2.3-2)$$

$$E\epsilon_z = -\mu S_x$$

whence

$$m = \frac{\epsilon_y}{\epsilon_x} = -\mu \quad (2.2-3)$$

Case (ii) Balanced Biaxial Differential Stress State

in which

$$\sigma_x = \sigma_y > \sigma_z \geq 0$$

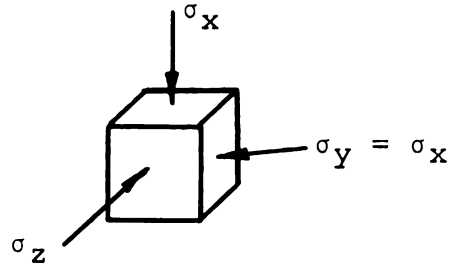


Fig. 2.6 Balanced Biaxial Differential Stress State

giving

$$\left[\begin{array}{ccc} S_x = (\sigma_x - \sigma_z) & - & - \\ - & S_y = (\sigma_y - \sigma_z) & - \\ - & - & S_z = 0 \end{array} \right] \quad (2.3-4)$$

$$\text{and } E\epsilon_x = S_x - \mu S_y = S_x(1 - \mu)$$

$$E\epsilon_y = S_y - \mu S_x = S_x(1 - \mu) \quad (2.5-3)$$

$$E\epsilon_z = -\mu(S_x + S_y) = -2\mu S_x$$

hence

$$m = \frac{\epsilon_y}{\epsilon_x} = 1 \quad (2.3-6)$$

Case (iii) General Biaxial Differential Stress State

in which

$$\sigma_x > \sigma_y > \sigma_z \geq 0$$

giving

$$\left[\begin{array}{ccc} S_x = (\sigma_x - \sigma_z) & - & - \\ - & S_y = (\sigma_y - \sigma_z) & - \\ - & - & S_z = 0 \end{array} \right] \quad (2.3-7)$$

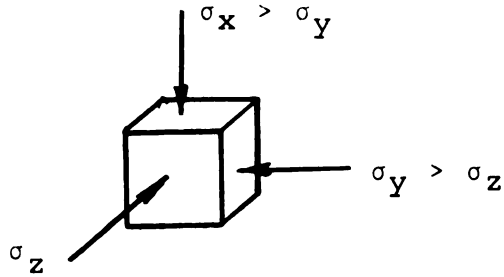


Fig. 2.7 General Biaxial Differential Stress State

$$\text{and } E\epsilon_x = S_x - \mu S_y$$

$$E\epsilon_y = S_y - \mu S_x \quad (2.3-8)$$

$$E\epsilon_z = -\mu(S_x + S_y)$$

hence

$$S_x = \frac{E}{1 - \mu^2} (\epsilon_x + \mu\epsilon_y) \quad (2.3-9)$$

but by equation 2.2-6

$$\epsilon_y = m\epsilon_x$$

and therefore

$$S_x = \frac{E(1 + m\mu)\epsilon_x}{1 - \mu^2} = E_{eq} \epsilon_x \quad (2.3-10)$$

where

$$E_{eq} = \frac{E(1 + m\mu)}{1 - \mu^2} \quad (2.3-11)$$

Equation 2.3-11 gives the relationship between the differential stress S_i and the differential strain ϵ_i for a general biaxial differential stress state. The change in the equivalent elastic constant E_{eq} with m is shown in Fig. 2.8.

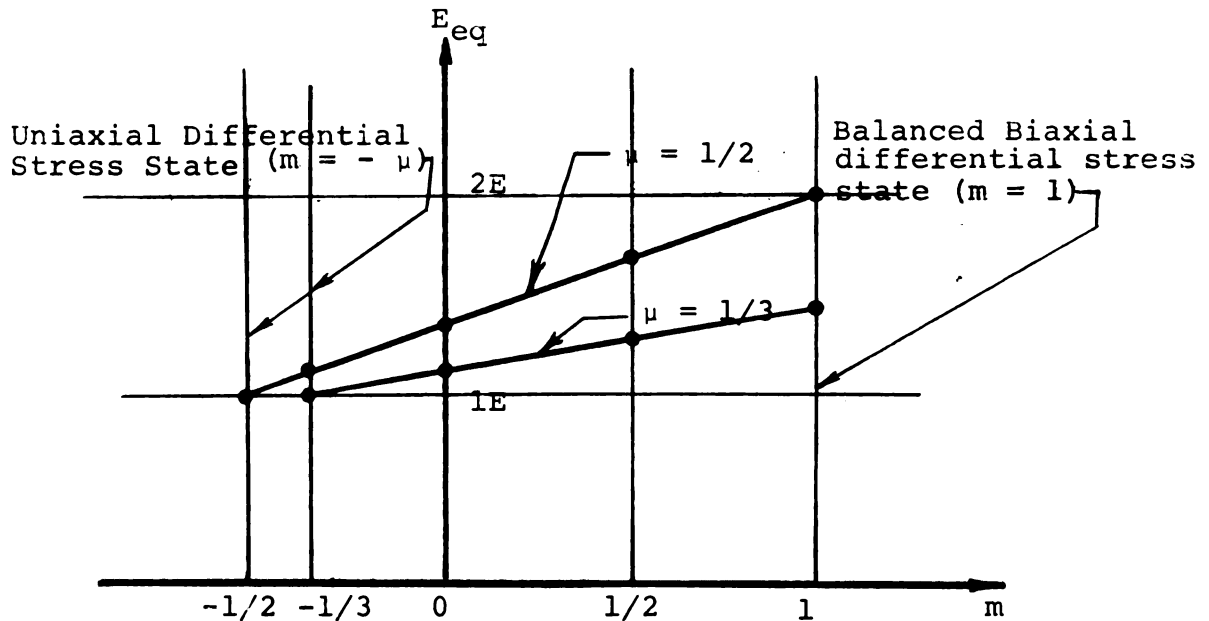


Fig. 2.8 Variation of E_{eq} with m

2.4 Behavior of Material Under Different Testing Conditions

It has been experimentally observed and verified (especially by Brace (1963)⁸ who ran tests on polished sections under dark field illumination) that for a certain constant rate of uniaxial loading an idealized stress-strain curve shows four characteristic stages as illustrated in Fig. 2.9.

In stages I and II the behavior is elastic; nearly all the strain is recoverable. The degree of curvature in stage I varies for different rocks, depending on their degree of porosity or compactness. In general, compact rocks have a straight stress-strain curve in this region whereas the loose rocks show rather pronounced curvature which disappears when

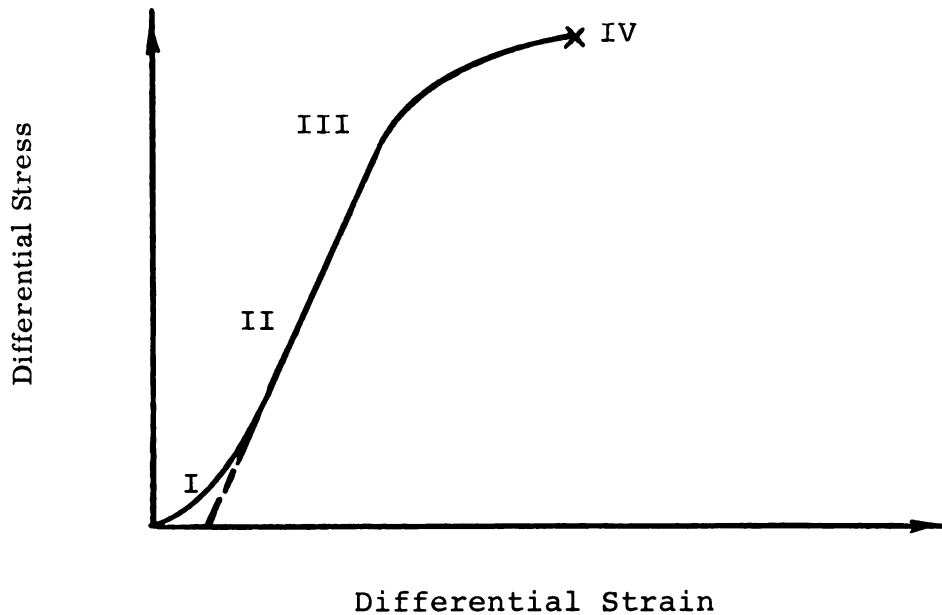


Fig. 2.9 Idealized Stress-Strain Diagram

and if a small hydrostatic pressure is applied to the specimen.

Starting with stage III, important permanent changes in the microscopic character of the compact rock occur. The rock takes a somewhat lighter color which was traced at high magnification to reflection of light at grain boundary surfaces. It was therefore apparent, that the crystal grains are becoming detached at their boundaries; and, when this occurs, the boundary becomes totally reflecting and therefore easily visible.

These reflecting surfaces become more numerous as fracture is approached in stage IV. However, this characteristic behavior in uniaxial deformation completely changes as soon as a confining pressure is applied; rock specimens cease to fail



Fig. 2.10 Failure of Rock Salt Specimen Tested Under Uniaxial Differential Stress with a Confining Pressure Equal to One Atmosphere

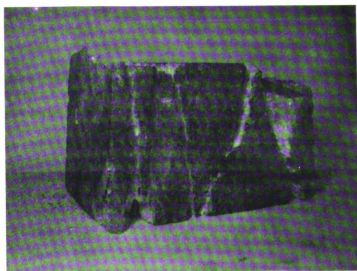


Fig. 2.11 Failure of Rock Salt Specimen Tested Under a Balanced Biaxial Differential Stress with a Confining pressure Equal to One Atmosphere

along the grain boundaries, and fracture takes place both in the crystals and their boundaries.

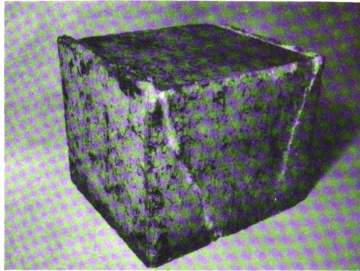


Fig. 2.12 Failure of Rock Salt Specimen Tested Under Uniaxial Differential Stress With a Confining Pressure Equal to One Hundred Atmospheres

These facts would indicate that:

(a) In a uniaxial differential stress test where the confining pressure is negligible, failure will occur when the differently oriented crystals tend to re-orient themselves in an effort to resist the applied differential stress; thus transmitting part of the load to the grain boundary layer or bond, and failure will ultimately occur when these bonds are destroyed.

(b) When a confining pressure is applied, the ability of the grains to reorient themselves will be restricted and hence a greater proportion of the imposed differential stress will be carried by the grains themselves rather than their being partially transmitted to the boundary.

The above physical characteristic behavior suggests that the inhomogeneous polycrystalline rocks are made up of two independent mechanical systems: (1) the grain boundary system and, (2) the composite crystal grain system, each of which will share the applied differential load in a proportion depending upon the degree of confinement.

CHAPTER III

THEORETICAL ANALYSIS

3.1 Proposed Rheological Model

Griggs (1939)¹⁶, Robertson (1960)³⁰ and other investigators have shown that the time-strain pattern exhibited by almost all polycrystalline rocks under a state of constant differential stress is similar to the curves shown in Fig. 3.1.

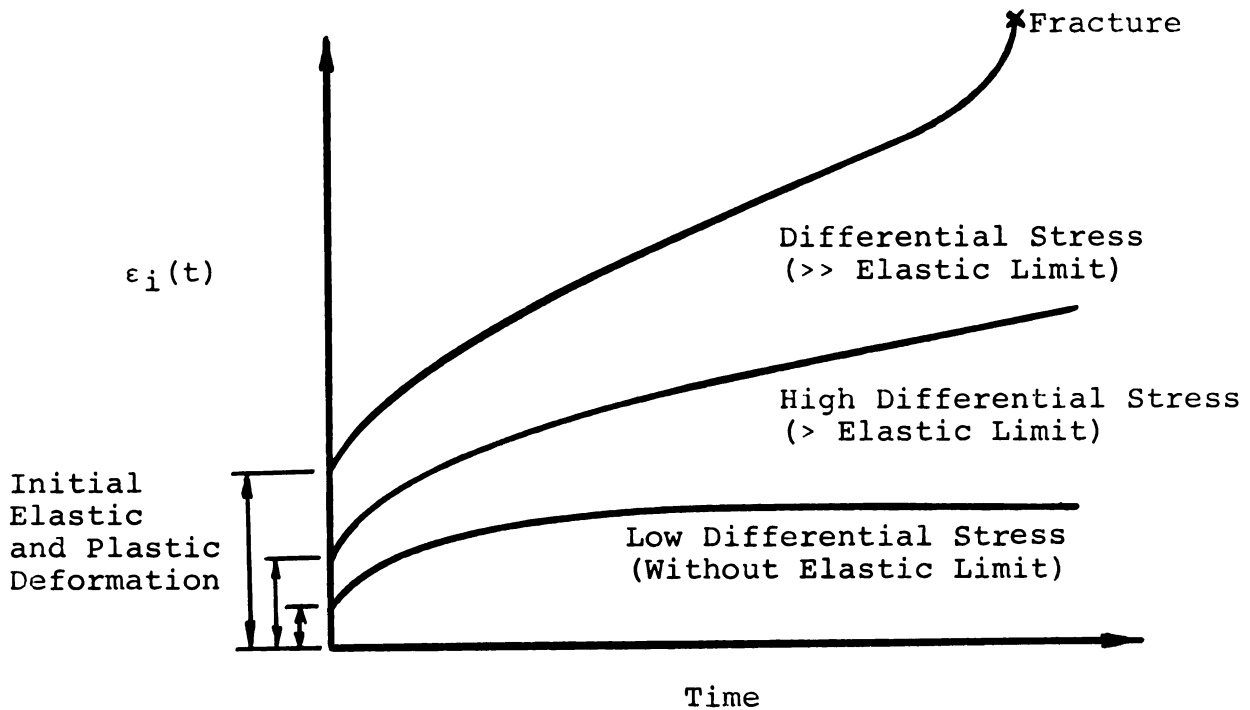


Fig. 3.1 Graph Representing the Different Creep Curves at Varying Magnitudes of Differential Stress

These curves exhibit an instantaneous elastic strain response which takes place upon the immediate application of the differential stress and is represented by OA in Fig. 3.2.

There follows a period of primary creep AB in which the rate of deformation decreases with time. Primary creep is sometimes referred to as delayed elastic deformation or visco-elastic flow, for if at any time T_1 the specimen is unloaded, there is first an elastic recovery BC followed by a time-elastic recovery represented by the curve CD.

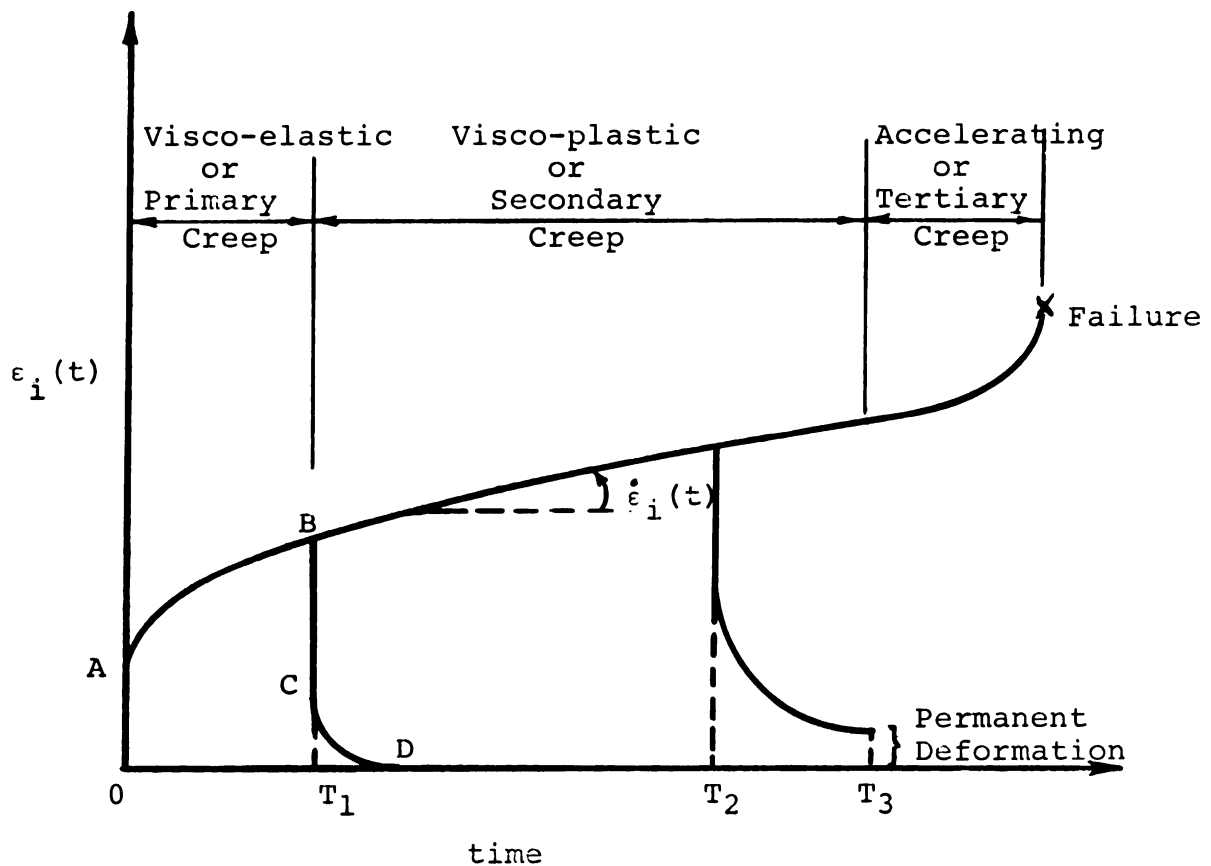


Fig. 3.2 Typical Creep Curve at Constant Differential Stress

However, if the load is not removed at time T_1 , and if the differential stress is greater than the elastic limit, the specimen begins to exhibit secondary creep, a phase of deformation in which the rate of strain is constant, whence the secondary creep is often called steady state creep.

Because the rate of strain is constant and because the specimen has undergone permanent deformation (as could be shown if the specimen was unloaded at time T_2) this deformation is also sometimes termed pseudo-viscous or visco-plastic creep.

Many empirical equations were introduced (as shown earlier by equations 1.2-1 and 1.2-2) in an effort to establish a relationship between the differential stress-differential strain-time elements which would fit experimental results; however, these equations do neither succeed in describing the full range of the experimental results nor do they account for the deformation mechanism of the material.

As a result, many investigators [e.g. Zener (1948)³³, Eirich (1956)¹¹ and Bland (1960)⁶] find it convenient to express the observed behavior of the material in terms of a mechanical model that is comprised of a number of simple units (for which the usual assumptions are made regarding isotropy and homogeneity).

One such model which can be used to interpret time-strain curves of this type is known as the visco-elastic or Burgers Model, (see Fig. 3.3). It mainly consists of a Maxwell unit coupled in series with a Voigt unit, in which the spring E represents the component of the body which gives rise to the instantaneous elastic strain.

The Voigt unit consisting of a spring and a dashpot coupled in parallel (E^* , n^*) represents the component responsible for primary or visco-elastic creep. The component

of secondary creep or visco-plastic flow is contributed by the dashpot η . However, this model will eventually exhibit permanent deformation even when the stress becomes exceedingly small, and therefore represents a viscous liquid.

In order to provide for a yield strength Y of the material which exists before attaining a steady state creep rate, a Bingham body is used to replace the dashpot of the Maxwell unit and is used in series with the spring and Voigt units. This new composite model is called The SVB (spring, Voigt, Bingham) Model, since there is no specific name given to it yet. As in the visco-elastic model, the spring E accounts for the instantaneous elastic deformation and the coupled spring and dashpot (E^* , η^*) accounts for the visco-elastic flow. However, before the visco-plastic deformation of the dashpot η can take place, the frictional resistance of the slider Y must be overcome. This frictional resistance in the model simulates the yield strength of the original substance.

Since polycrystalline rocks are inhomogeneous and have rather displayed the existence of two separate systems, the following mechanical model (Fig. 3.5) is introduced not only to relate the strain-time relationship as a function of the differential stress but also as a function of the confining pressure.

The model consists of a grain boundary system and a crystal grain system in parallel; each system is represented

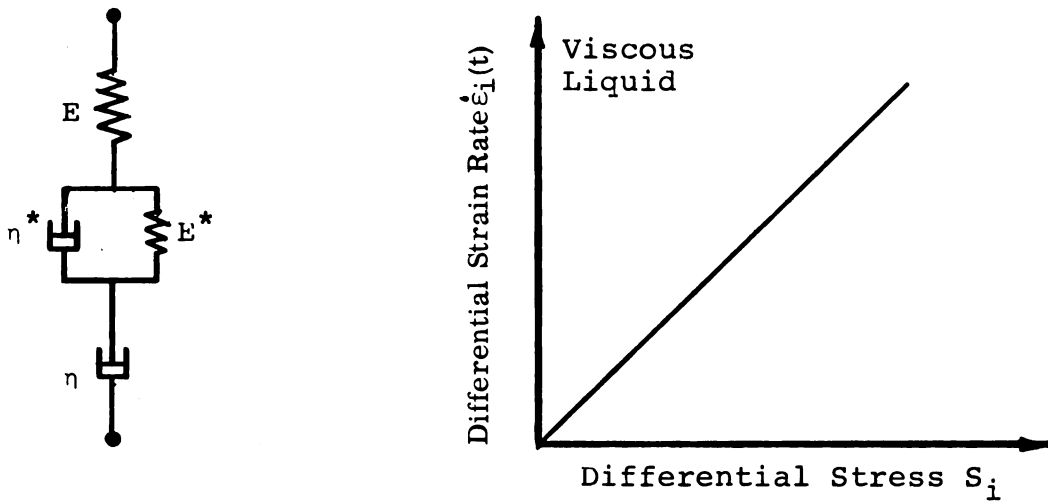


Fig. 3.3 Burgers Model showing the relationship between differential strain rate and differential stress for the steady-state or visco-plastic creep.

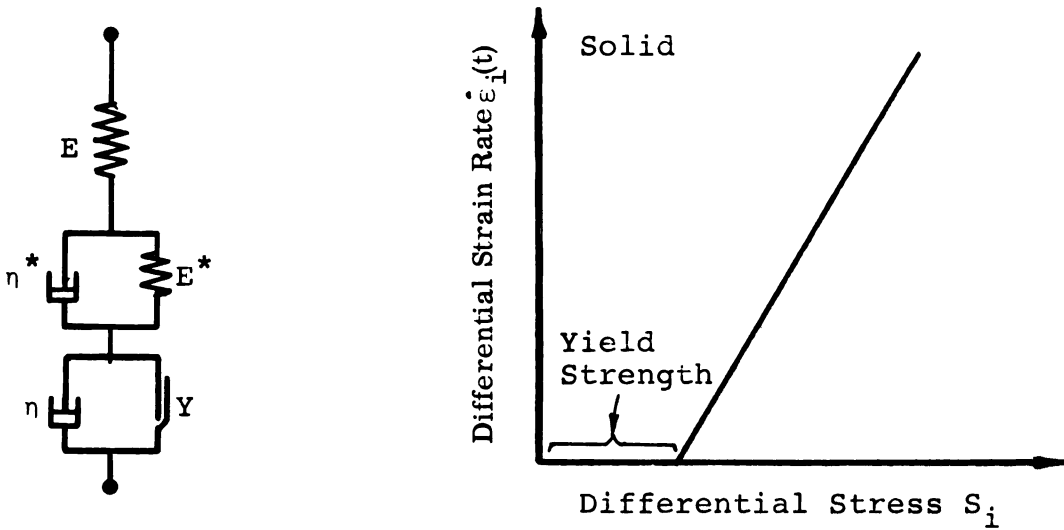


Fig. 3.4 SVB Model showing the relationship between differential strain rate and differential stress for the steady-state or visco-plastic creep.

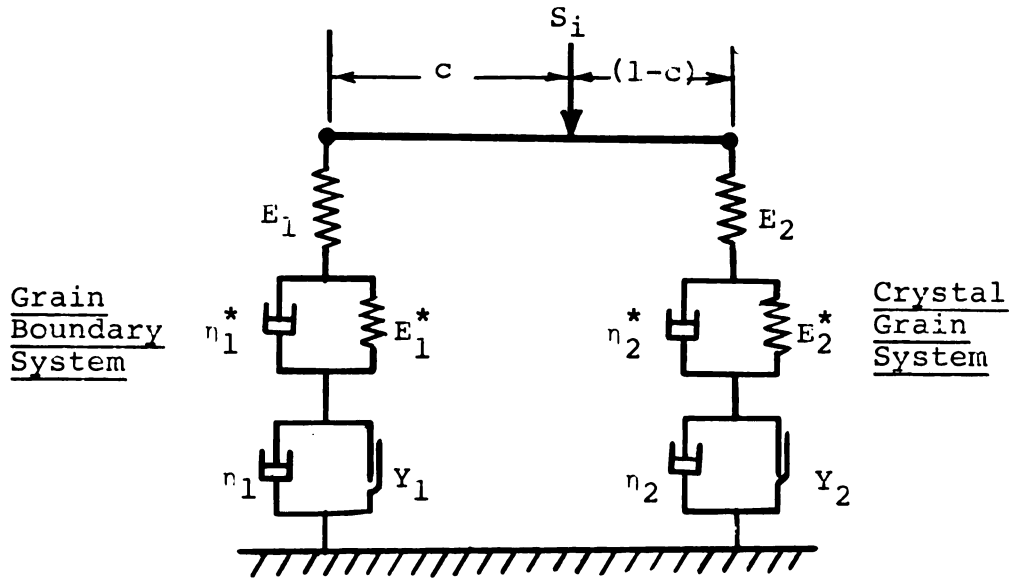


Fig. 3.5 Proposed Mechanical Model

as an SVB model fixed at the bottom to a rigid base. At the top, the two systems are coupled together by a rigid bar hinged to each system, while the position of the applied differential stress S_i along the hinged bar relative to the two systems varies according to the degree of confining pressure c .

3.2 Assumptions

(i) The element constants shown in the proposed model representing the properties of the aggregate material are statistical averages of the properties of the crystals and their boundaries taken over all orientations.

(ii) Specimens sufficiently large to contain enough crystal grains are assumed to be statistically isotropic.

(iii) The crystal grain elements' constants are always the same for a certain type of polycrystalline material; however, the grain boundary elements' constants might differ for the same material, depending on the previous temperature and stress history to which the specimens have been subjected.

(iv) The effect of a hydrostatic principal stress tensor ($\sigma_x = \sigma_y = \sigma_z$) on the deformation of polycrystalline rock is assumed to be linearly elastic and to have negligible variation with time. Thus it can be represented by the equation

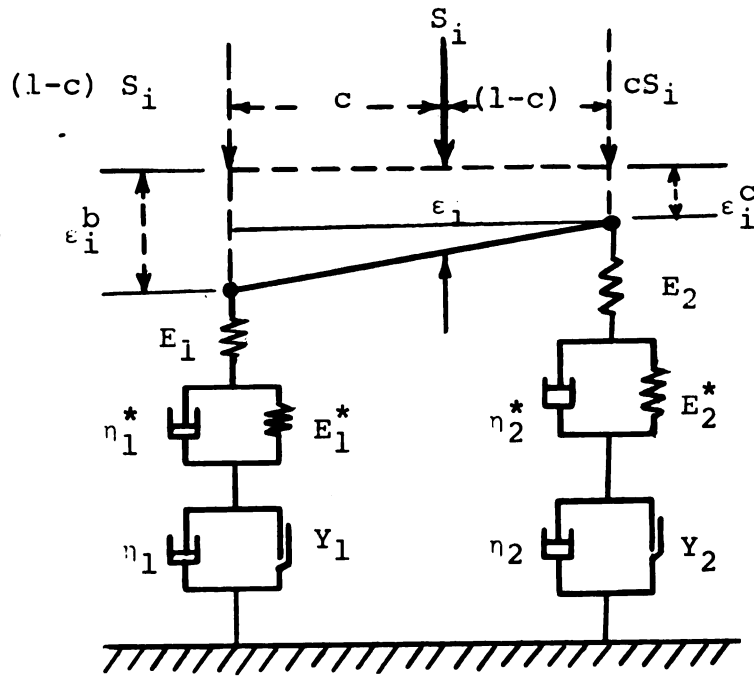
$$\sigma_i = G \epsilon_i'' = \frac{E}{1-2\mu} \epsilon_i'' \quad (3.2-1)$$

where G is the hydrostatic elastic constant of the material.

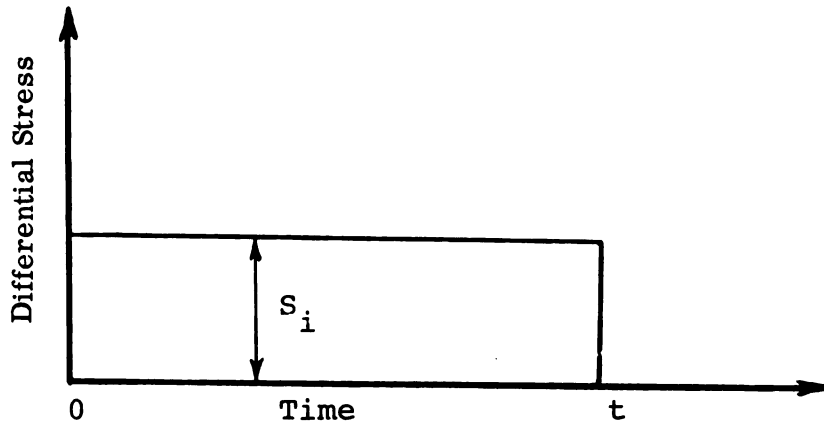
3.3 Variation of Behavior with Confining Pressure

The relationship between differential stress S_i and differential strain ϵ_i and the degree of confinement c is determined by utilizing the proposed rheological model (Fig. 3.6-a with a history of loading as shown in Fig. 3.6-b) in which

- E_1, E_1^* = Elastic constants of grain boundary bonds
- η_1^*, η_1 = Visco-Elastic and visco-plastic coefficients of bonds
- Y_1 = Differential yield strength of boundary bonds
- S_i^b = Applied differential stress on boundary system
- ϵ_i^b = Differential strain of boundary system
- E_2, E_2^* = Elastic constants of crystal grains



(a) Deformation of Model due to applied differential stress



(b) History of Loading

Fig. 3.6 Differential Stress-Strain-Time Relationship

η_2^* , η_2 = Visco-elastic and visco-plastic coefficients of grains

Y_2 = Differential Yield strength of grains

S_i^C = Applied differential stress on grains

ϵ_i^C = Differential strain of grains

t = Time

From the equilibrium of the rigid bar,

$$S_i^C = c S_i \quad (3.3-1)$$

$$S_i^b = (1 - c) S_i$$

and from the compatibility condition of the two systems

$$\epsilon_i = \epsilon_i^C + (1 - c) (\epsilon_i^b - \epsilon_i^C) = (1 - c) \epsilon_i^b + c \epsilon_i^C \quad (3.3-2)$$

but $\epsilon_i^C = [\epsilon_{i1}^C]$ elastic + $[\epsilon_{i2}^C]$ visco-elastic

$$+ [\epsilon_{i3}^C] \text{ visco-plastic} \quad (3.3-3)$$

and by considering the constitutive relationship of the three elements, it follows that:

$$(i) \epsilon_{i1}^C = c S_i \left(\frac{1}{E_2} \right) \quad (3.3-4)$$

$$(ii) \eta_2^* \frac{d\epsilon_{i2}^C}{dt} + E_2^* \epsilon_{i2}^C = c S_i$$

$$\text{or } \frac{d\epsilon_{i2}^C}{dt} + \frac{E_2^*}{\eta_2^*} \epsilon_{i2}^C = \frac{c}{\eta_2^*} S_i$$

and by using the integration factor $e^{\frac{E_2^*}{\eta_2^*} t}$, we get

$$\frac{d}{dt} \left(\epsilon_{i2}^C e^{\frac{E_2^*}{\eta_2^*} t} \right) = \frac{c S_i}{\eta_2^*} e^{\frac{E_2^*}{\eta_2^*} t}$$

$$\text{or } \epsilon_{i2}^C e^{\frac{E_2^*}{\eta_2^*} t} = \frac{c}{\eta_2^*} S_i \int e^{\frac{E_2^*}{\eta_2^*} t} dt$$

assuming that $\epsilon_{i2}^C = 0$ at $t = 0$.

Therefore

$$\epsilon_{i2}^C = c S_i \left[\frac{1}{E_2^*} \left(1 - e^{-\frac{E_2^* t}{n_2^*}} \right) \right] \quad (3.3-5)$$

$$(iii) \quad c S_i = Y_2 + n_2 \frac{d\epsilon_{i3}^C}{dt} \quad (\text{if } c S_i > Y_2)$$

$$\text{or } \frac{d\epsilon_{i3}^C}{dt} = \frac{1}{n_2} (c S_i - Y_2)$$

$$\text{or } \epsilon_{i3}^C = \frac{c S_i}{n_2} \left(1 - \frac{Y_2}{c S_i} \right) \int_0^t dt$$

assuming $\epsilon_{i3}^C = 0$ at $t = 0$.

Therefore

$$\epsilon_{i3}^C = c S_i \left(1 - \frac{Y_2}{c S_i} \right) \frac{t}{n_2} \quad (3.3-6)$$

Hence, by substituting equations 3.3-4, 3.3-5 and 3.3-6 into equation 3.3-3, we obtain

$$\begin{aligned} \epsilon_i^C = c S_i \left\{ \left[\frac{1}{E_2} \right] + \right. \\ \left. + \left[\frac{1}{E_2^*} \left(1 - e^{-\frac{E_2^* t}{n_2^*}} \right) \right] + \left[\left(1 - \frac{Y_2}{c S_i} \right) \frac{t}{n_2} \right] \right\} \end{aligned} \quad (3.3-7a)$$

Similarly, it can be shown that

$$\begin{aligned} \epsilon_i^b = (1 - c) S_i \left\{ \left[\frac{1}{E_1} \right] + \left[\frac{1}{E_1^*} \left(1 - e^{-\frac{E_1^* t}{n_1^*}} \right) \right] \right. \\ \left. + \left[\left(1 - \frac{Y_1}{(1 - c) S_i} \right) \frac{t}{n_1} \right] \right\} \end{aligned} \quad (3.3-7b)$$

By substituting equations 3.3-7a and 3.3-7b into equation 3.3-2, we get the general relationship

$$\begin{aligned} \epsilon_i = S_i \left\{ (1 - c)^2 \left[\frac{1}{E_1} + \frac{1}{E_1^*} \left(1 - e^{-\frac{-E_1^* t}{\eta_1^*}} \right) \right. \right. \\ \left. \left. + \left(1 - \frac{Y_1}{(1 - c) S_i} \right) \frac{t}{\eta_1} \right] + c^2 \left[\frac{1}{E_2} + \frac{1}{E_2^*} \left(1 - e^{-\frac{-E_2^* t}{\eta_2^*}} \right) \right. \right. \\ \left. \left. + \left(1 - \frac{Y_2}{c S_i} \right) \frac{t}{\eta_2} \right] \right\} \end{aligned} \quad (3.3-8)$$

which can be written as

$$\epsilon_i = S_i \left\{ \left[\frac{(1 - c)^2}{E_1} + \frac{c^2}{E_2} \right] \right.$$

representing the equivalent elastic response

$$\left. + \left[\frac{(1 - c)^2}{E_1^*} \left(1 - e^{-\frac{-E_1^* t}{\eta_1^*}} \right) + \frac{c^2}{E_2^*} \left(1 - e^{-\frac{-E_2^* t}{\eta_2^*}} \right) \right] \right\}$$

representing the equivalent visco-elastic response (3.3-8a)

$$\left. + \left[\frac{(1 - c)^2 t}{\eta_1} \left(1 - \frac{Y_1}{(1 - c) S_i} \right) + \frac{c^2 t}{\eta_2} \left(1 - \frac{Y_2}{c S_i} \right) \right] \right\}$$

representing the equivalent visco-plastic response

3.3a Variation of the equivalent elastic response with the degree of confinement

From the derived general relationship (equation 3.3-8),

it was shown that

$$\frac{1}{E_{eq}} = \frac{(1-c)^2}{E_1} + \frac{c^2}{E_2}$$

If we let $E_2 = \alpha E_1$ (3.3-9)

we get
$$\frac{1}{E_{eq}} = \frac{(1-c)^2}{E_1} + \frac{c^2}{\alpha E_1}$$

or
$$E_{eq} = \frac{\alpha E_1}{c^2 + \alpha(1-c)^2}$$
 (3.3-10)

Maximizing equation 3.3-10 with respect to c , we obtain

$$\frac{d(E_{eq})}{dc} = \frac{-\alpha E_1 [2c - 2\alpha(1-c)]}{[c^2 + \alpha(1-c)^2]^2} = 0$$

from which we find that $(E_{eq})_{max}$ occurs at

$$c = \frac{\alpha}{1 + \alpha}$$
 (3.3-11)

Hence $(E_{eq})_{max} = (1 + \alpha) E_1 = E_1 + E_2$ (3.3-12)

Also when $E_{eq} = E_2 = \alpha E_1$, a quadratic equation of c is obtained giving

$$c^2 + \alpha(1-c)^2 - 1 = 0$$
 (3.3-13)

which could be re-arranged as

$$[(\alpha + 1)c - (\alpha - 1)][c - 1] = 0$$

with two roots: $c = 1$ and $c = \frac{\alpha - 1}{\alpha + 1}$

A typical curve showing the variation of E_{eq} with the degree of confinement c is shown in Fig. 3.7 for the particular

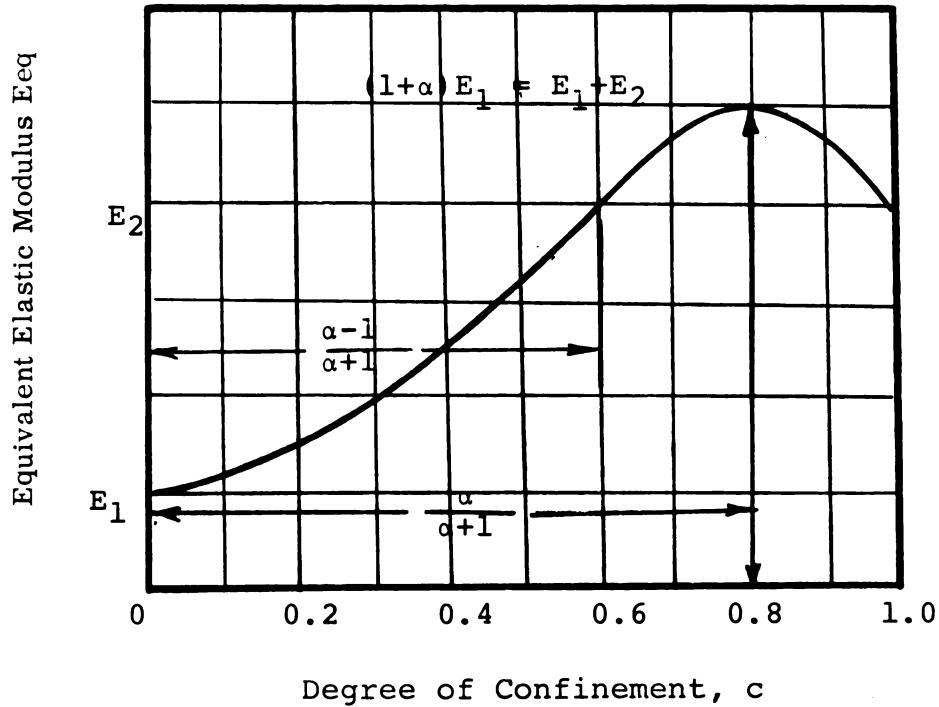


Fig. 3.7 Typical Variation of E_{eq} with c

value of $\alpha = 4$; while in the next two pages, the calculations (Table 3.1) and a graph (Fig. 3.8) showing this same variation for various values of α are presented.

3.3b Variation of the equivalent visco-elastic response with the degree of confinement

The visco-elastic creep response as obtained by the derived general expression (equation 3.3-8) was shown to be:

$$\epsilon_i(t) = S_i \left[\frac{(1-c)^2}{E_1^*} \left(1 - e^{\frac{-E_1^* t}{\eta_1^*}}\right) + \frac{c^2}{E_2^*} \left(1 - e^{\frac{-E_2^* t}{\eta_2^*}}\right) \right]$$

$\alpha \backslash c$	0.1	0.2	0.3	0.4	0.5	0.6	0.7	0.8	0.9	1.0
1	1.22E ₂	1.47E ₂	1.72E ₂	1.92E ₂	2.0 E ₂	1.92E ₂	1.72E ₂	1.47E ₂	1.22E ₂	E ₂
2	0.61E ₂	0.76E ₂	0.93E ₂	1.14E ₂	1.33E ₂	1.47E ₂	1.49E ₂	1.39E ₂	1.20E ₂	E ₂
3	0.41E ₂	0.52E ₂	0.64E ₂	0.81E ₂	1.00E ₂	1.19E ₂	1.32E ₂	1.32E ₂	1.19E ₂	E ₂
4	0.31E ₂	0.38E ₂	0.49E ₂	0.63E ₂	0.80E ₂	1.00E ₂	1.18E ₂	1.25E ₂	1.18E ₂	E ₃
5	0.25E ₂	0.31E ₂	0.39E ₂	0.51E ₂	0.67E ₂	0.86E ₂	1.06E ₂	1.19E ₂	1.16E ₂	E ₂
6	0.21E ₂	0.26E ₂	0.33E ₂	0.43E ₂	0.57E ₂	0.76E ₂	0.97E ₂	1.14E ₂	1.15E ₂	E ₂
7	0.18E ₂	0.22E ₂	0.28E ₂	0.37E ₂	0.50E ₂	0.68E ₂	0.89E ₂	1.09E ₂	1.14E ₂	E ₂
8	0.15E ₂	0.19E ₂	0.25E ₂	0.33E ₂	0.44E _s	0.61E ₂	0.83E ₂	1.04E ₂	1.12E ₂	E ₂
9	0.14E ₂	0.17E ₂	0.22E ₂	0.29E ₂	0.40E ₂	0.56E ₂	0.77E ₂	1.00E ₂	1.11E ₂	E ₂
10	0.12E ₂	0.16E ₂	0.20E ₂	0.27E ₂	0.36E ₂	0.51E ₂	0.72E ₂	0.96E ₂	1.10E ₂	E ₂

Table 3.1 Calculations of E_{eq} vs c for different values of α

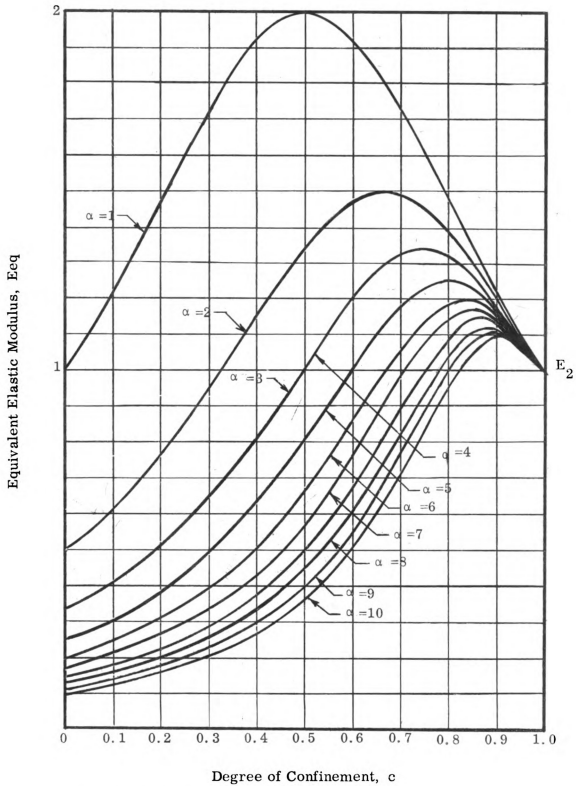


Fig. 3.8. Variation of E_{eq} vs. c for various values of α .

If we let $E_2^* = \alpha^* E_1^*$ (3.3-14)

then $\epsilon_i(t) = S_i \left\{ \left[\frac{\alpha^* (1-c)^2}{E_2^*} + \frac{c^2}{E_2^*} \right] - \left[\frac{\alpha^* (1-c)^2}{E_2^*} e^{-\frac{E_1^* t}{\eta_1^*}} \right. \right.$

$$\left. \left. + \frac{c^2}{E_2^*} e^{-\frac{E_2^* t}{\eta_2^*}} \right] \right\}$$
 (3.3-15)

By denoting

$$\frac{E_2^*}{\eta_2^*} = \frac{1}{\tau_2}$$
 (3.3-16)

and $\frac{E_1^*}{\eta_1^*} = \frac{\beta^*}{\tau_2}$

then $\frac{\eta_2^*}{\eta_1^*} = \alpha^* \beta^*$ (3.3-16a)

By substituting equations 3.3-16 into equations 3.3-15, we obtain

$$\epsilon_i(t) = \frac{S_i}{E_2^*} \left\{ [c^2 + \alpha^* (1-c)^2] + [c^2 e^{-\frac{t}{\tau_2}} \right.$$

$$\left. + \alpha^* (1-c)^2 e^{-\frac{\beta^* t}{\tau_2}} \right] \right\}$$

which can be rewritten as

$$\epsilon_i(t) = \frac{S_i}{E_2^*} \left\{ [c^2 + \alpha^* (1-c)^2] + \sqrt{\alpha^* c^2 (1-c)^2} e^{-\frac{t}{2\tau_2}(\beta^* + 1)} \right. \\ \left. \left[\sqrt{\frac{c^2}{\alpha^* (1-c)^2}} e^{\frac{t}{2\tau_2}(\beta^* - 1)} + \sqrt{\frac{\alpha^* (1-c)^2}{c^2}} e^{-\frac{t}{2\tau_2}(\beta^* - 1)} \right] \right\}$$

or

$$\epsilon_i(t) = \frac{S_i}{E_2^*} \left\{ [c^2 + \alpha^* (1-c)^2] + \sqrt{\alpha^* c (1-c)} e^{-\frac{t}{2\tau_2}(\beta^* + 1)} \right.$$

$$\left. \left[e^{\frac{1}{2} \log \frac{c^2}{\alpha^* (1-c)^2}} e^{\frac{1}{2} \frac{t}{\tau_2} (\beta^* - 1)} \right. \right.$$

$$\left. \left. + e^{-\frac{1}{2} \log \frac{c^2}{\alpha^* (1-c)^2}} e^{-\frac{t}{2\tau_2}(\beta^* - 1)} \right] \right\}$$

or

$$\epsilon_i(t) = \frac{S_i}{E_2^*} \left\{ [c^2 + \alpha^* (1-c)^2] + 2\sqrt{\alpha^* c (1-c)} e^{-\frac{t}{2\tau_2}(\beta^* + 1)} \right.$$

$$\left. \cosh \frac{1}{2} \left[(\beta^* - 1) \frac{t}{\tau_2} + \log \frac{c^2}{\alpha^* (1-c)^2} \right] \right\} \quad (3.3-17)$$

This relationship between $\epsilon_i(t)$ and t is illustrated by the curve shown in Fig. 3.9, in which the expected creep range

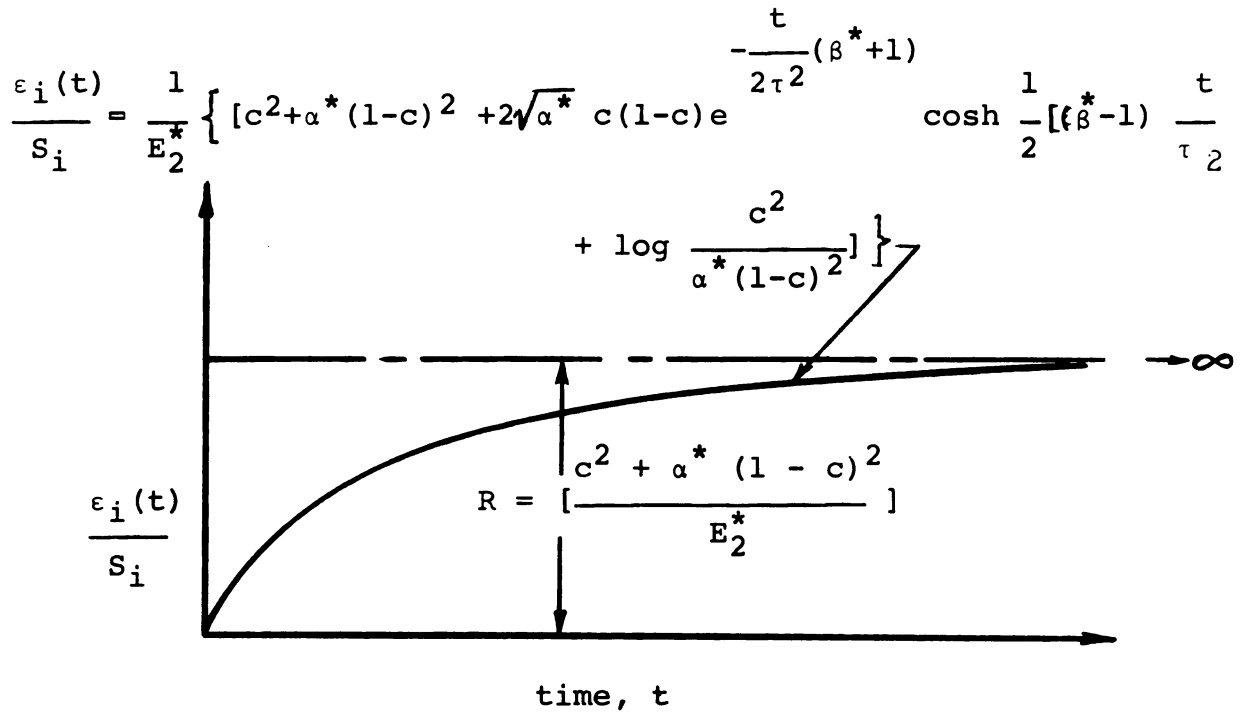


Fig. 3.9 Variation of the Visco-elastic Creep with time

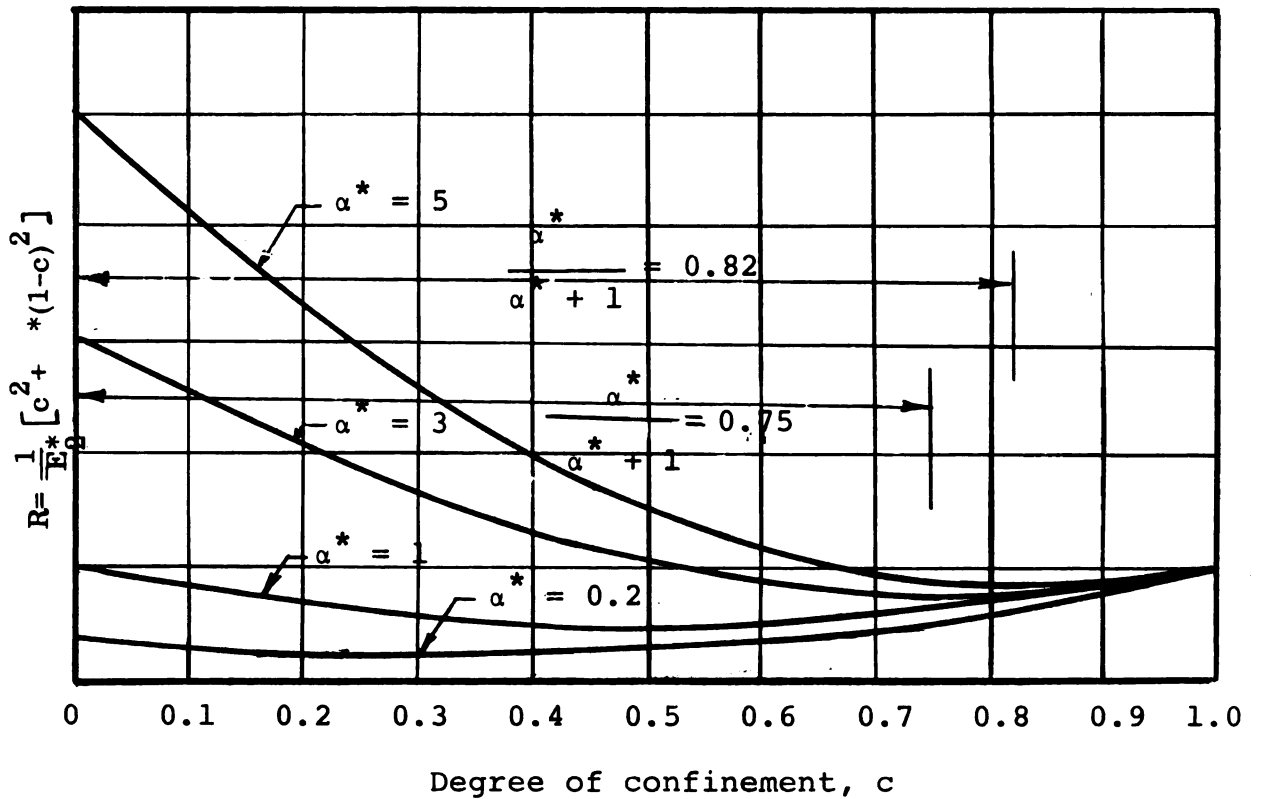


Fig. 3.10 Variation of the Range with the degree of confinement

R is the value approached by $\epsilon_i(t)/S_i$ as $t \rightarrow \infty$, given by

$$\frac{\epsilon_i(\infty)}{S_i} = R = \frac{1}{\frac{E^*}{2}} [c^2 + \alpha^* (1-c)^2] \quad (3.3-18)$$

The variations of the range R with the degree of confinement c is shown in Fig. 3.10, and is dependent on the value of α^* . It is worthwhile to note that the range is always an increasing function of c when c is sufficiently near to 1.

Thus, by finding the appropriate values of β^* and τ , almost any visco-elastic creep behavior can be approximated, after determining the approximate value of α^* from the preceding range analysis. To illustrate this characteristic change in behavior, consider for simplicity, the variation of the visco-elastic creep curves with the degree of confinement c in the following two cases:

$$\begin{array}{ll} \text{Case (a)} & \alpha^* = 1 \\ & \tau = 2 \\ & \beta^* = 1 \\ \text{Case (b)} & \alpha^* = 1 \\ & \tau = 2 \\ & \beta^* = 5 \end{array}$$

By examining the two plots of cases (a) and (b) shown in figures 3.11 and 3.12 respectively, we see that because α^* in both cases was chosen to be the same and equal to 1, the ranges of the visco-elastic curves were equal for the same c. However, by changing β^* , the ratio of β^*/τ has been changed causing a change in the dependence of the initial slope on c.

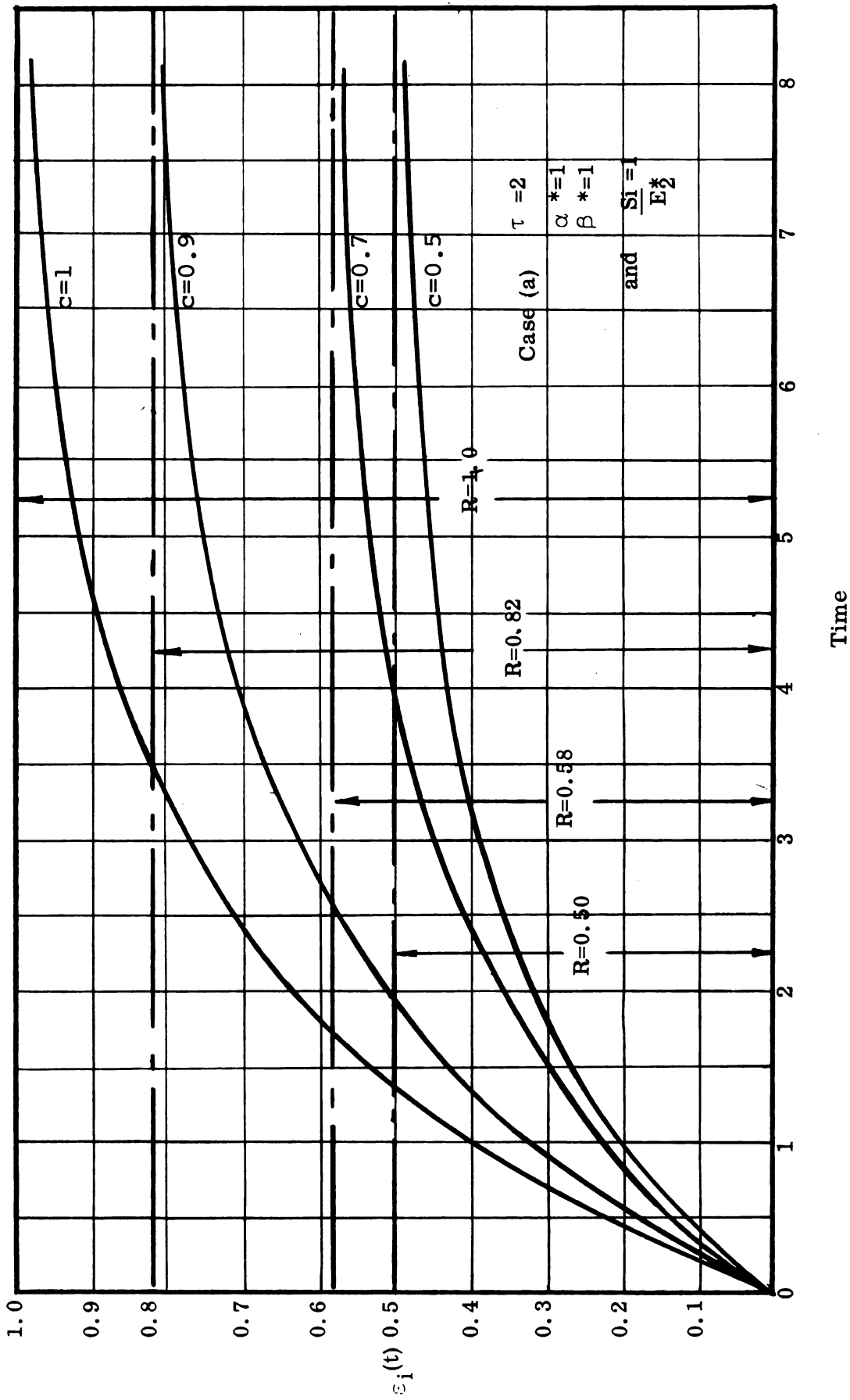


Fig. 3.11. Variation of Visco-elastic Creep with the Degree of Confinement for Case (a).

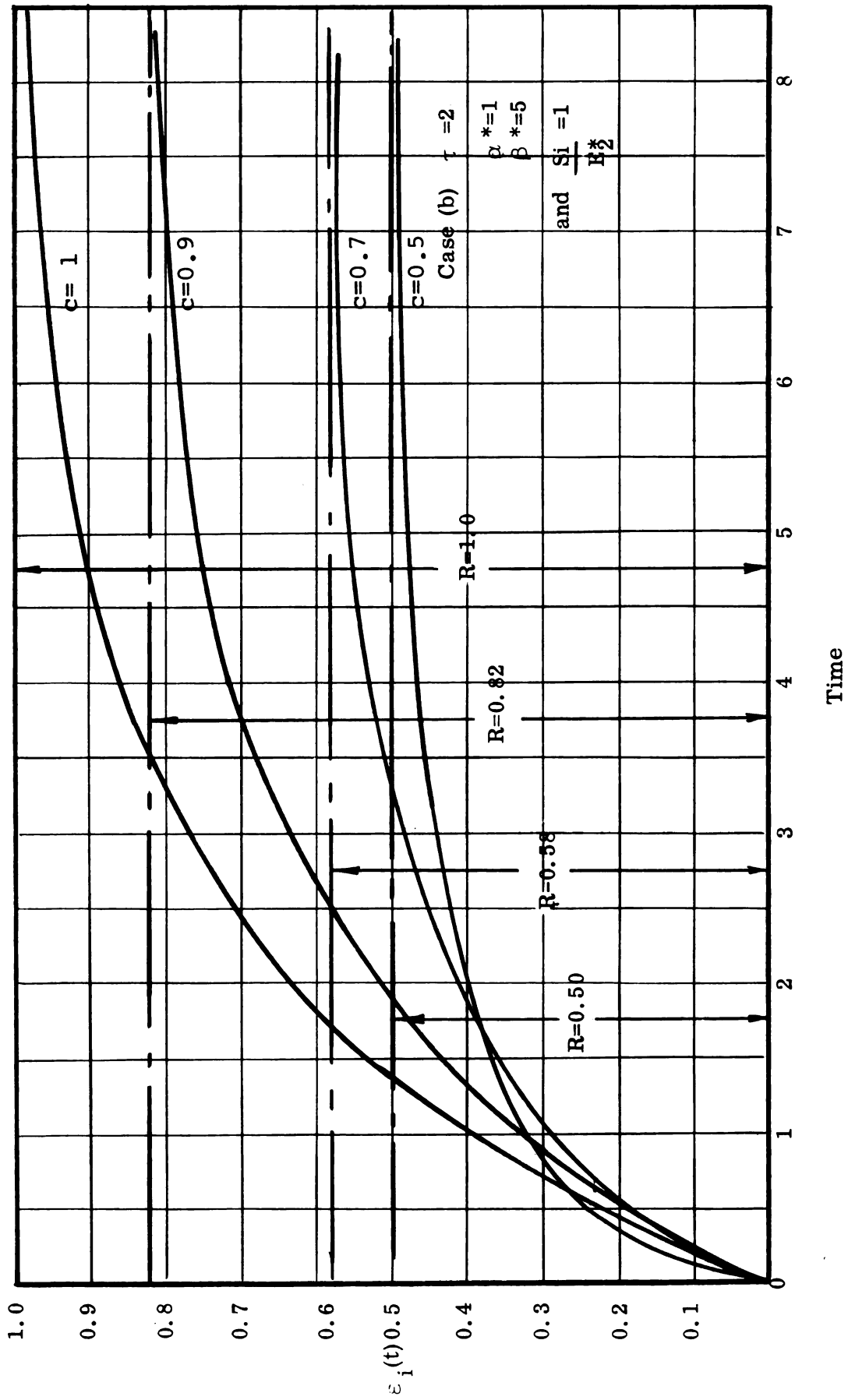


Fig. 3.12 Variation of Visco-elastic Creep with the Degree of Confinement for Case (b).

In case (a) the initial slope increased as c increased, while in case (b) the initial slope first decreased and then increased as c approached 1.

3.3c Variation of the equivalent visco-plastic response with the degree of confinement

The visco-plastic response derived from the general solution of the proposed model (equation 3.3-8) was given as

$$\epsilon_i(t) = S_i t \left[\frac{(1-c)^2}{\eta_1} \left(1 - \frac{Y_1}{(1-c) S_i}\right) + \frac{c^2}{\eta_2} \left(1 - \frac{Y_2}{c S_i}\right) \right]$$

provided that

$$c S_i > Y_2$$

$$\text{and } (1-c) S_i > Y_1$$

now if we let

$$\frac{\eta_2}{\eta_1} = \beta$$

(3.3-19)

$$\frac{Y_2}{Y_1} = \lambda$$

and substitute equations 3.3-19 into the above equation, we

obtain

$$\epsilon_i(t) = \frac{S_i t}{\eta_2} \left[\beta(1-c) \left(1 - c - \frac{Y_2}{\lambda S_i}\right) + c \left(c - \frac{Y_2}{S_i}\right) \right]$$

$$\text{or } \epsilon_i(t) = \frac{S_i t}{\eta_2} \left[\beta(1-c)^2 + c^2 - \frac{Y_2}{S_i} \left(c + \frac{\beta(1-c)}{\lambda}\right) \right]$$

$$\text{or } \epsilon_i(t) = \frac{S_i t}{\eta_2} \left\{ \beta(1-c)^2 + c^2 - \frac{Y_2}{S_i} \left[c \left(1 - \frac{\beta}{\lambda}\right) + \frac{\beta}{\lambda} \right] \right\} \quad (3.3-20)$$

Again to illustrate the change in the steady state slope of the creep curve with the degree of confinement, we choose for simplicity an example in which $\beta/\lambda = 1$, and therefore, the visco-plastic response becomes

$$\epsilon_i(t) = \frac{S_i t}{\eta_2} \left[\beta (1 - c)^2 + c^2 - \frac{Y_2}{S_i} \right] \quad (3.3-21)$$

from which the steady state slope of the creep curve is obtained by differentiating $\epsilon_i(t)$ with respect to t , thus getting

$$\eta_2 \dot{\epsilon}_i(t) = S_i \left[\beta (1 - c)^2 + c^2 - \frac{Y_2}{S_i} \right] \quad (3.3-22)$$

which when plotted for a constant c and varying S_i will give a straight line relationship as shown in figure 3.13.

In order to plot the variation of the differential strain rate with the degree of confinement c , it is noticed that the behavior will depend on the value of β , which is expected to be much less than 1, since it is experimentally observed that the grain boundary is much more viscous than the actual crystal grains themselves. This fact has been observed even in metals and verified by Kê (1947)²² in a set of experiments on polycrystalline and single aluminum crystals, in which aluminum wire was used in a torsion pendulum oscillating at a constant frequency. Kê found a relaxation peak in the internal friction when measured at different temperatures for polycrystalline aluminum which was not observed when single aluminum crystals were tested, and concluded that the phenomenon was primarily due to the high viscosity of the grain boundaries.

Thus if we assume an arbitrary value for Y_2/S_i and a

value of β less than 1, a decrease in the initial part of the curve showing strain rate with the degree of confinement (Fig. 3.14) is observed, followed by an increase as c tends to approach 1.

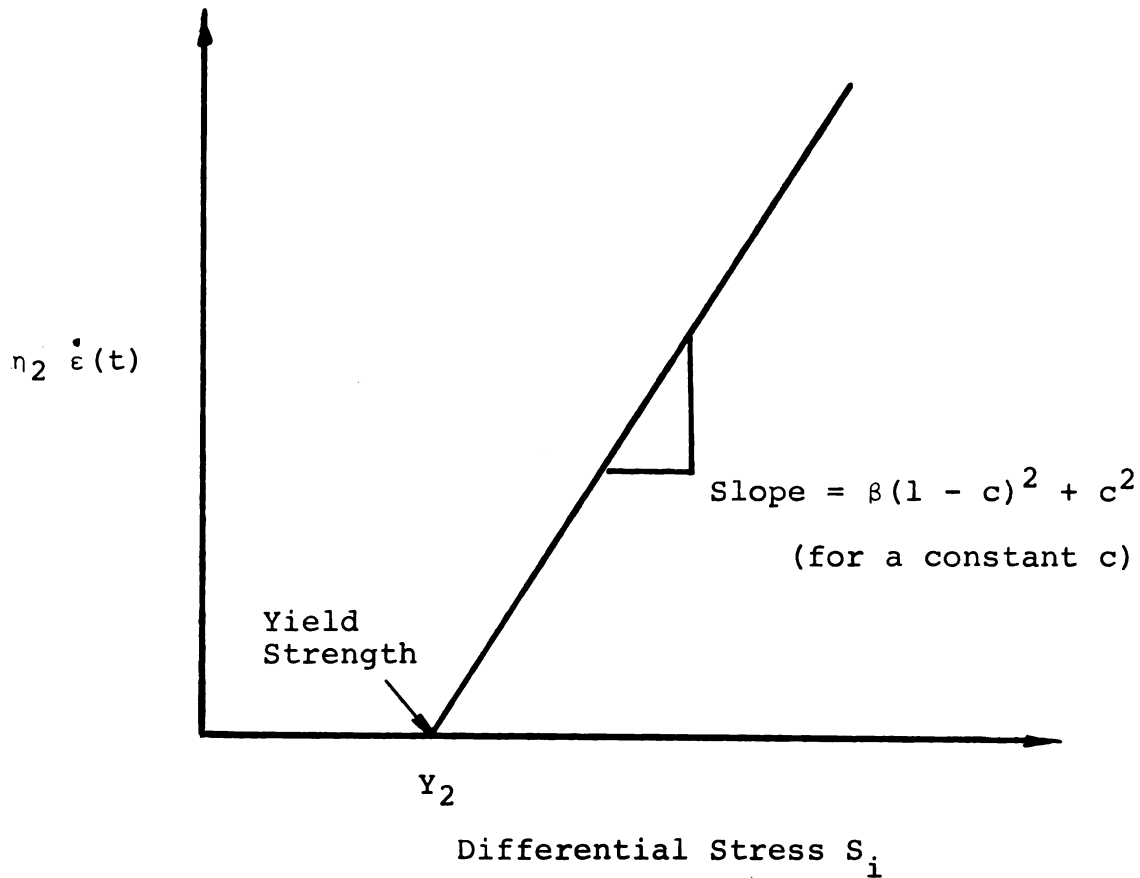


Fig. 3.13 Relationship Between Differential Strain Rate and Differential Stress for the Steady State Response

The value of c corresponding to the minimum value of the differential strain rate is obtained by differentiating $\dot{\epsilon}_i(t)$ with respect to c

$$\frac{d \dot{\epsilon}_i(t)}{d c} = \frac{S_i}{n_2} [-2 \beta (1 - c) + 2c] = 0$$

Hence

$$2c (\beta + 1) = 2\beta$$

$$\text{or } (c)_{\min} = \frac{\beta}{\beta + 1} \quad (3.3-23)$$

for the case when $\beta = \lambda$.

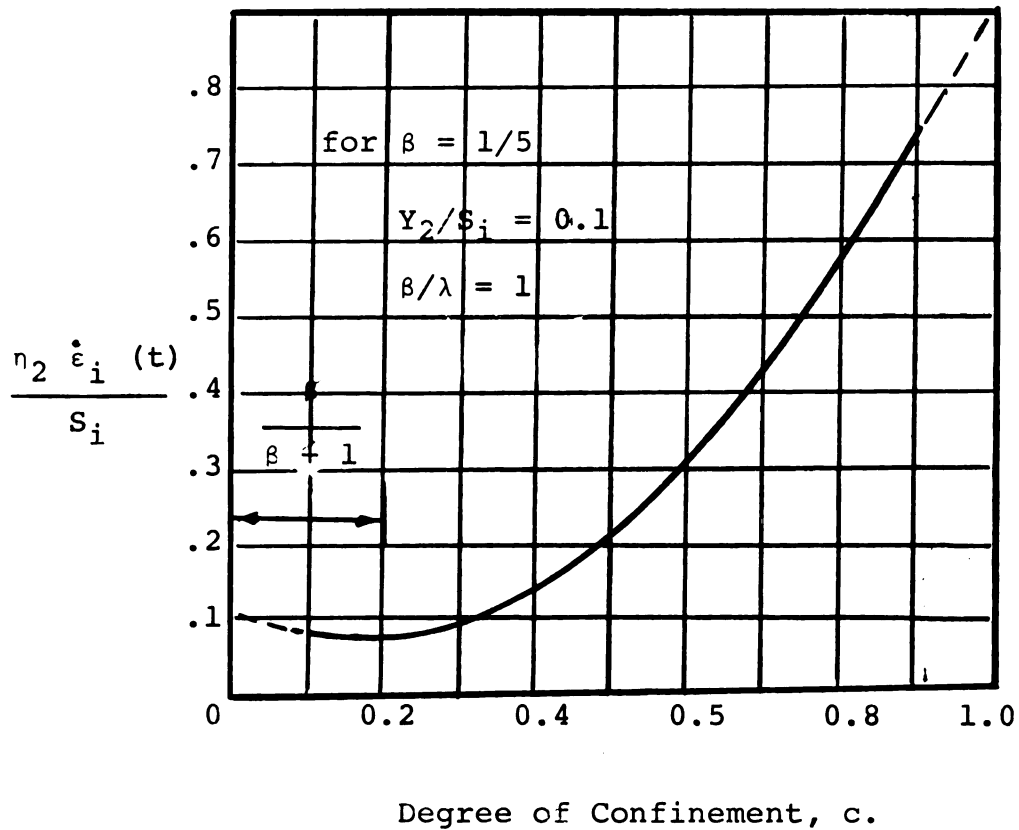


Fig. 3.14 Relationship Between Differential Strain Rate and Degree of Confinement

CHAPTER IV

APPLICATION AND PREDICTIONS OF THEORY

From most of the work that has been done to relate the five factors affecting the behavior of polycrystalline rock, all that can be concluded is that there exists some sort of variation in the behavior; since, up to the present time, no theoretical basis to guide investigators has been established.

As a result, only a very few regular and systematic tests have been performed using a relatively wide range of experimental variation to demonstrate the influence of confining pressure and temperature. These will be utilized here to show how the experimental results could be compared with the theoretical solution obtained by utilizing the proposed mechanical model if the proper values of the different elements were known.

4.1 Variation of the Elastic Modulus E_{eq} with Confining Pressure

After experiments done by Griggs (1936)¹⁵, Handin (1953¹⁸ and 1957¹⁹), Heard (1960)²⁰, Brace (1963)⁸ and Baron (1963)⁵, it has become an established fact that an increase in confining pressure tends to increase the elastic modulus. This could be explained by the fact that confining pressure raises the activation energy of the crystal grains that constitute the skeleton of the rock by restricting their displacement or re-orientation.

Nevertheless, Heard (1960)²⁰ and Baron (1963)⁵ working with confining pressure up to 5,000 Kg/cm² were surprised to get an increase in the elastic modulus with an initial increase in the confining pressure followed by a decrease of the elastic modulus with a subsequent increase in the confining pressure.

Such a behavior can easily be explained by examining the solution of the proposed model as demonstrated by the following two examples:

Example 1: Results of differential stress versus differential strain of rock salt specimens at different constant confining pressures were presented by Handin (1953)¹⁸ (Fig. 4.1). These results demonstrate the increase of the elastic modulus with the degree of confining pressure. Upon

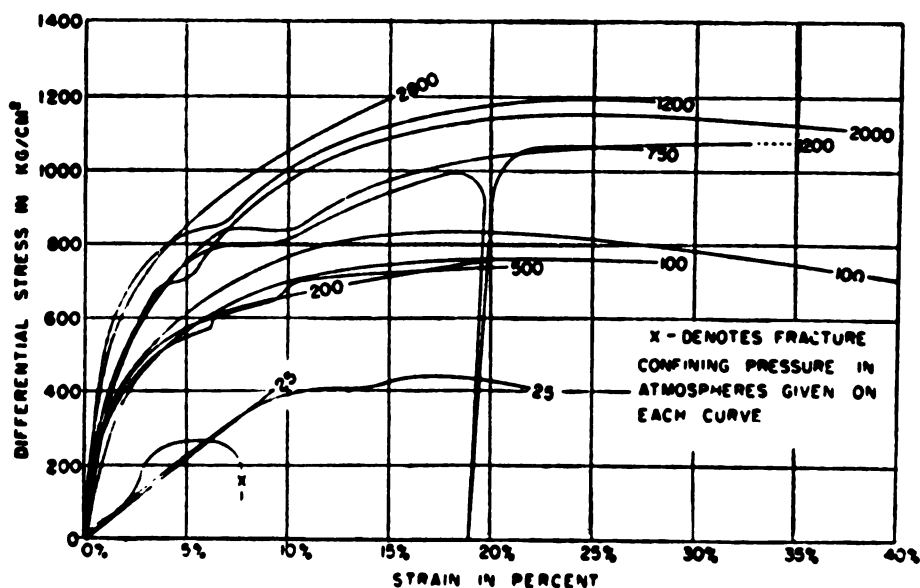


Fig. 4.1 Differential Stress-Strain Curves of Rock Salt Specimens Deformed in Compression (After J. Handin (1953)¹⁸)

measuring the initial elastic modulus, one finds the following values

$$E_{25} = 4,500 \text{ Kg/cm}^2$$

$$E_{100} = 24,000 \text{ Kg/cm}^2$$

$$E_{2000} = 42,000 \text{ Kg/cm}^2$$

$$E_{2800} = 63,000 \text{ Kg/cm}^2$$

A fitting method was used to determine the best possible values of the springs E_1 and E_2 that could represent the same variation. To do this, one must first assume what the expected maximum value of E_{eq} would have been had the test been run for the full range. This value of $(E_{eq})_{max}$ is equal to the sum of E_1 and E_2 as was shown previously. Again if E_2 is not known, a feasible value of E_2 is guessed and hence the ratio of the two springs α is determined from these assumed values. By knowing the value of α , a curve is plotted for the experimental values of E_{eq} versus the degree of confinement c , utilizing table 3.1. The actual points (E_{eq}, p) are then plotted over this theoretically determined curve in an effort to establish the relationship between the relative degree of confinement, c , and the actual confining pressure, p . If no fit is obtained between the two curves, a new set of spring values should be assumed, and the same procedure is repeated until a close fit between the theoretical and actual variation is obtained.

For this particular example, it is found that by using

$$E_1 = 9,000 \text{ kg/cm}^2$$

$$E_2 = 63,000 \text{ kg/cm}^2$$

$$\alpha = 7$$

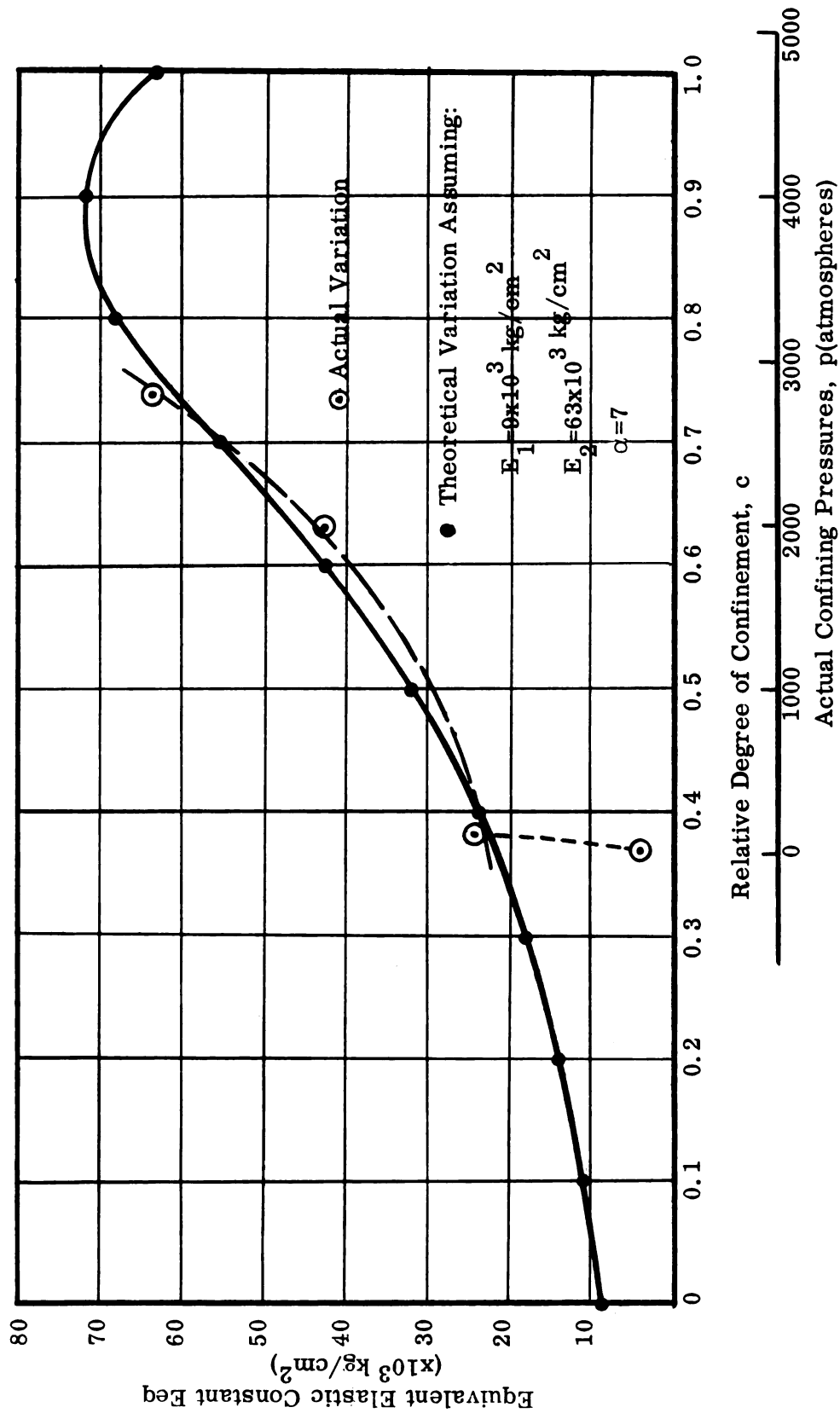


Fig. 4.2. Graph of E_{eq} vs. p for Rock Salt at Constant Room Temperature.

a close agreement between most of the theoretical and actual values is obtained (Fig. 4.2).

Example 2: Heard (1960)²⁰ presented results of differential stress versus strain curves at constant confining pressures for Solenhofen Limestone specimens, at a constant room temperature of 25°C as shown in Fig. 4.3.

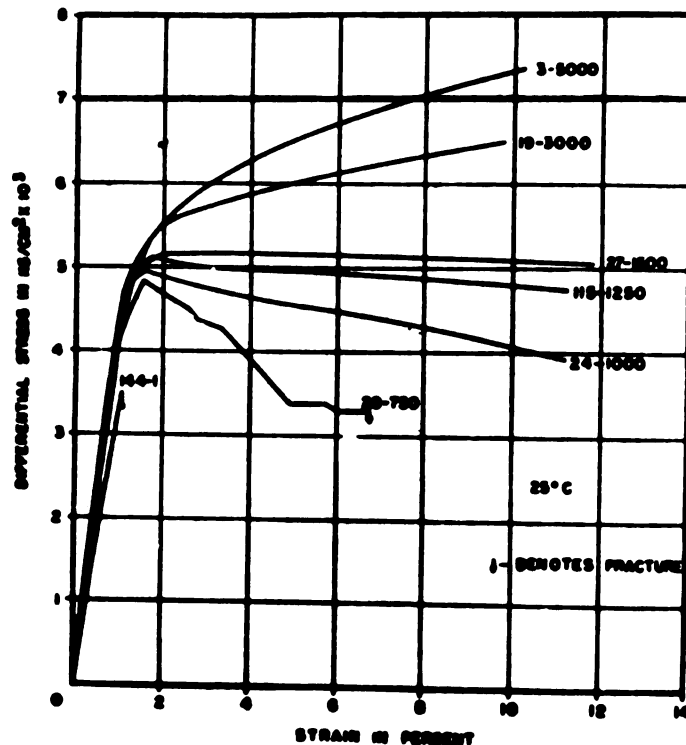


Fig. 4.3 Differential Stress-Strain Curves for Solenhofen Limestone (After H. C. Heard)²⁰

From these curves, the following initial elastic moduli were obtained.

$$E_1 = 3.25 \times 10^5 \text{ kg/cm}^2$$

$$E_{3000} = 4.65 \times 10^5 \text{ kg/cm}^2$$

$$E_{5000} = 4.20 \times 10^5 \text{ kg/cm}^2$$

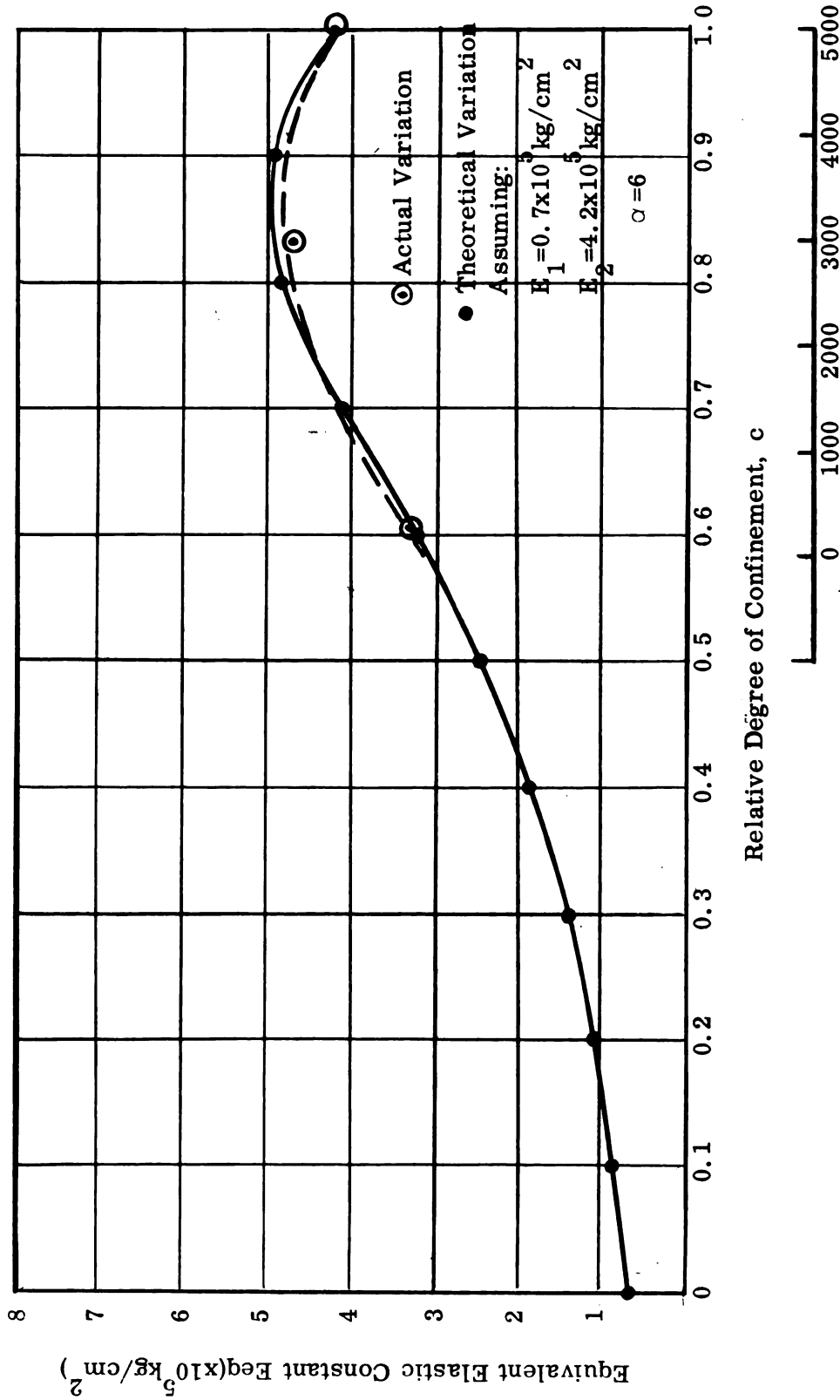


Fig. 4.4. Graph of E_{eq} . vs. p for Solenhofen Limestone at a Constant Room Temperature of 25°C .

Again, the same method of fitting is applied and by assuming a value of $E_2 = 4.20 \times 10^5 \text{ kg/cm}^2$

$$E_1 = 0.70 \times 10^5 \text{ kg/cm}^2$$

$$\alpha = 6$$

a close fit is obtained as shown in Fig. 4.4.

It is worthwhile to note the linear variation of the degree of confinement c with the confining pressure p in each of the above two examples.

4.2 Variation of the Visco-Elastic Range with Confining Pressure

Creep experiments using polycrystalline rock were first started by Griggs (1939)¹⁶ in an effort to investigate the variation that takes place for various combinations of the five influencing factors, and as a result some empirical relationships were suggested.

Robertson (1960)²⁸ has presented the only systematic creep work; his work was on Solenhofen Limestone at different levels of constant differential stress, different confining pressures, and at constant room temperature. Some of his plots are shown in Fig. 4.5. Several empirical relationships were suggested in an effort to establish a correlation between the differential stress-differential strain-time elements, and it was concluded that a more theoretical approach is certainly needed to relate these variables and improve the planning of creep experiments.

Price (1964)²⁶ and others have recently applied model analysis to some creep tests on rocks. However, since they

used a single system model, it was only applied satisfactorily to the behavior in the uniaxial state of stress.

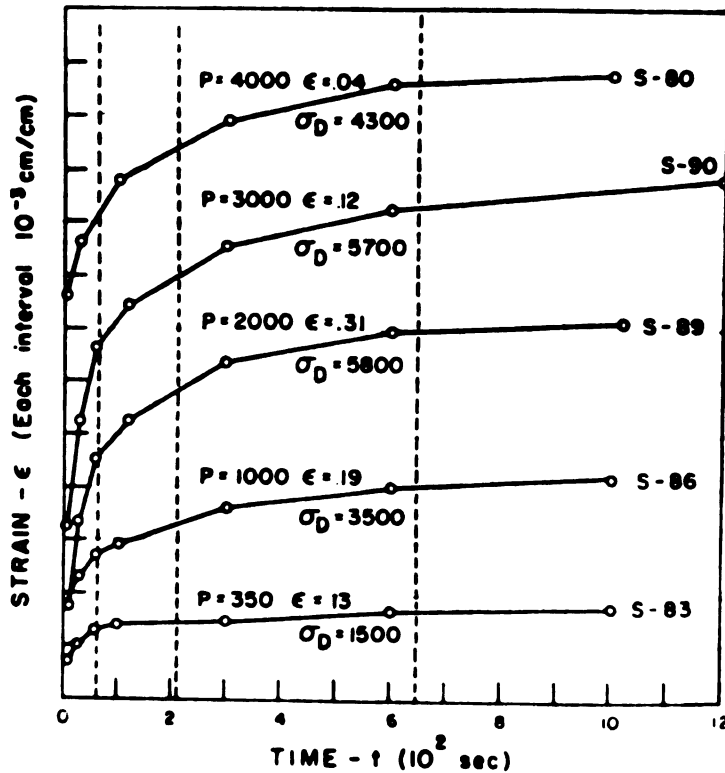


Fig. 4.5 Creep Test Results on Solenhofen Limestone Specimens (After E.C. Robertson²⁸)

In analysing the work of Robertson which is replotted in Fig. 4.6, the following two assumptions are made:

- (i) The visco-plastic creep is negligible, or has not begun during the whole analysis of the visco-elastic response.
- (ii) The visco-elastic response is negligible (or has been completed) during the steady-state creep.

Curves (i), (ii) and (iii) in Fig. 4.6, representing the visco-elastic creep response (since their differential stress level is within the elastic limit) are normalized

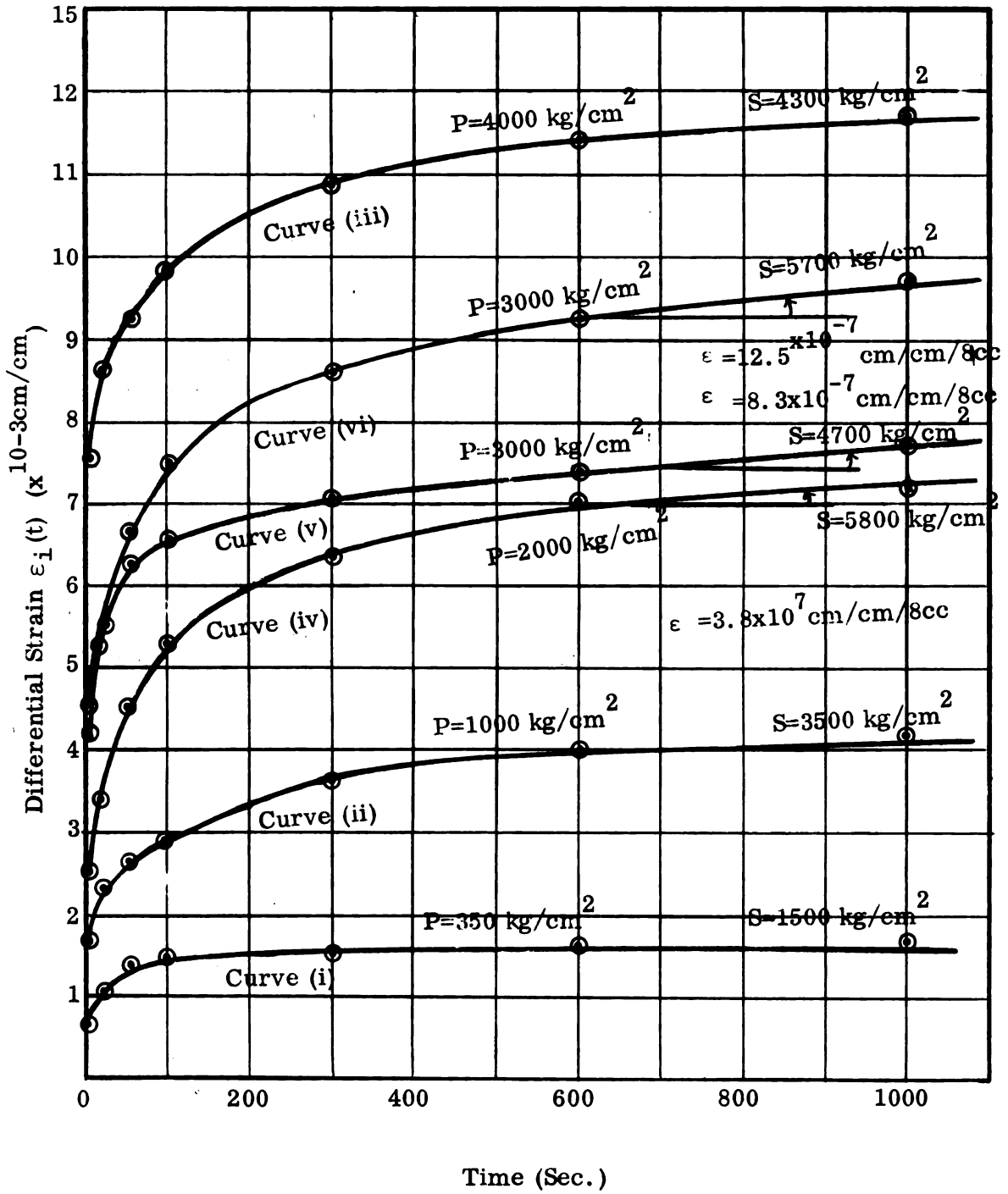


Fig. 4.6. Creep Test Results on Solenhofen Limestone [after Robertson (1960)²⁸]

to the same differential stress level of curve (i) by reducing their respective differential strain ordinate in the ratio of the differential stress of curve (i) to the differential stress of the respective curve. The normalized curves are plotted in Fig. 4.7, and for comparison, they are again plotted in Fig. 4.8 after being reduced to the same origin.

The range of each of these three curves is then estimated by making a reasonable assumption for the ordinate approached as $t \rightarrow \infty$. The estimated ranges are plotted versus the degree of confinement c (since the relationship of the actual confining pressure p to the degree of confinement c has already been established from the earlier elastic analysis) as shown in Fig. 4.9.

By assuming what the maximum range would have been at $c = 1$, the usual method of fitting is applied to determine (by trial and error) the best value of α^* to give the closest fit. In this particular example, it has been found that if

$$\alpha^* = 1$$

$$\text{and the maximum range} = 2.2 \times 10^{-3} \text{ cm/cm}$$

$$(\text{at } c = 1)$$

a close fit is obtained.

Thus, it is worthwhile to note that by observing the variation in behavior as obtained from experimental results of systematic tests, the values of the elements of the grain boundary system can be roughly determined if the exact values of the elements of the crystal grain system have already been established.

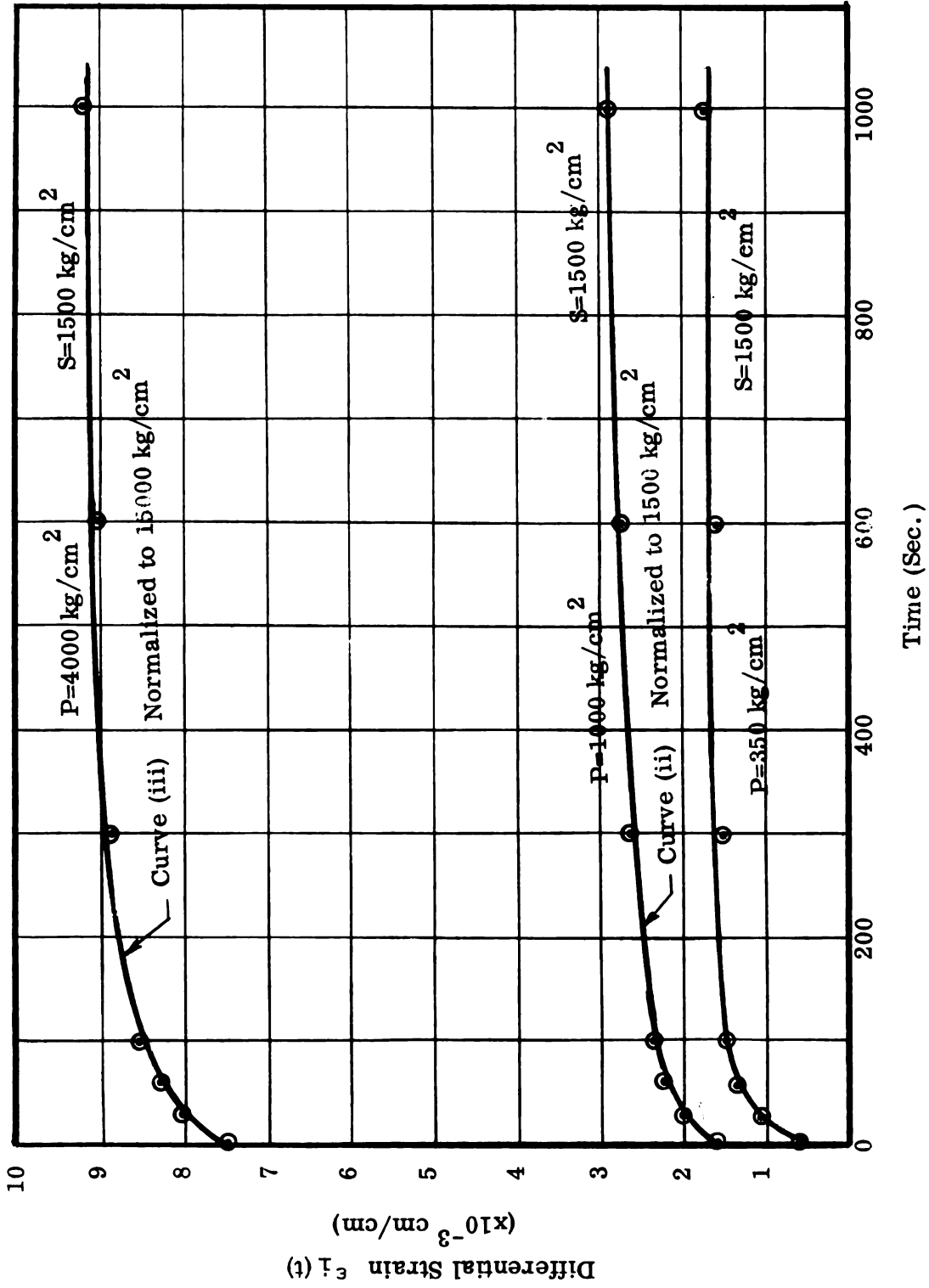


Fig. 4.7. Normalized Visco Elastic Creep Curves of Solenhofen Limestone at Different Confining Pressures and Same Differential Stress.

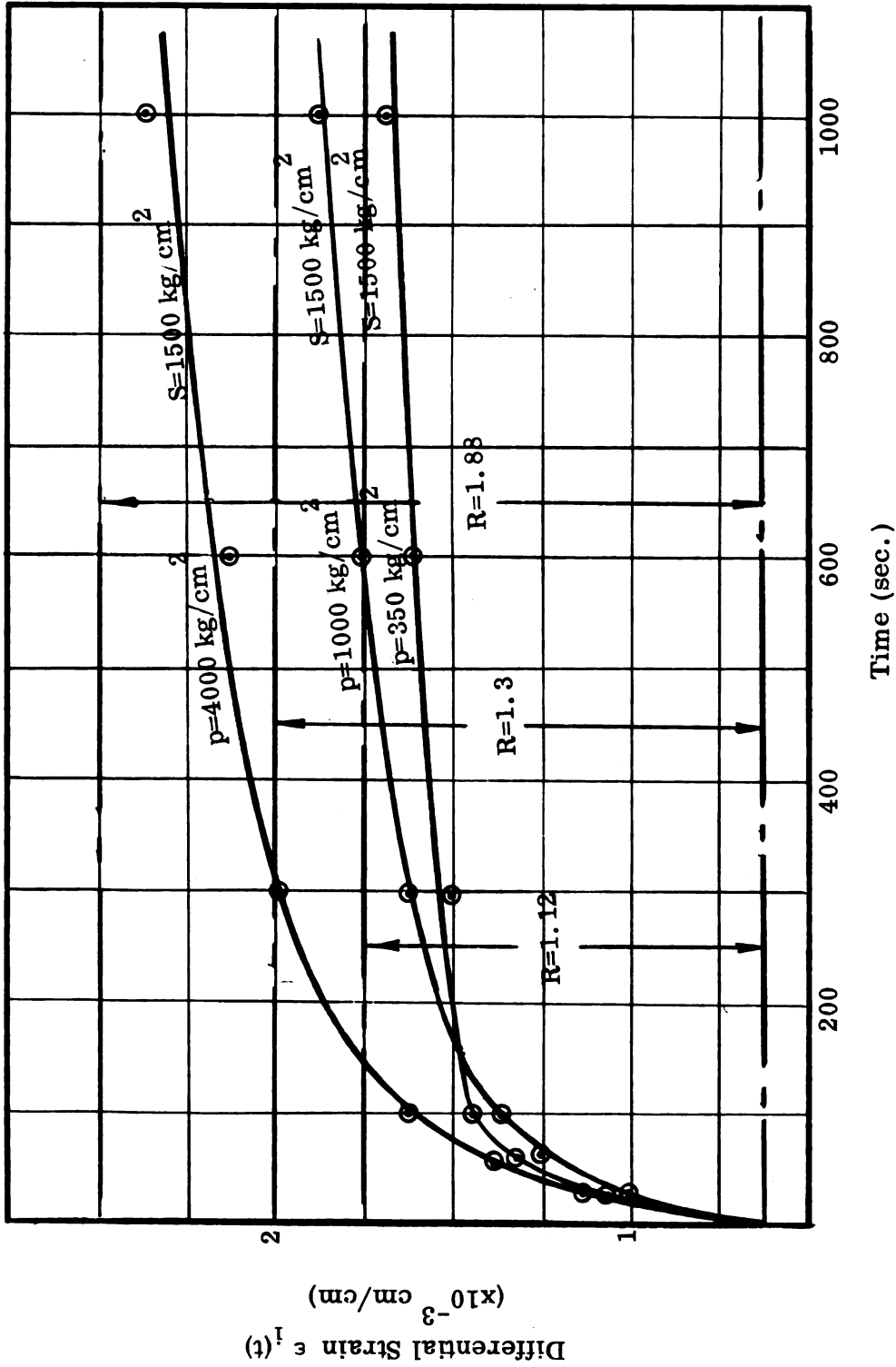


Fig. 4.8. Comparison of the Effect of Confining Pressure on the Range and initial slope of the Visco-elastic Curves of Solenhofen Limestone.

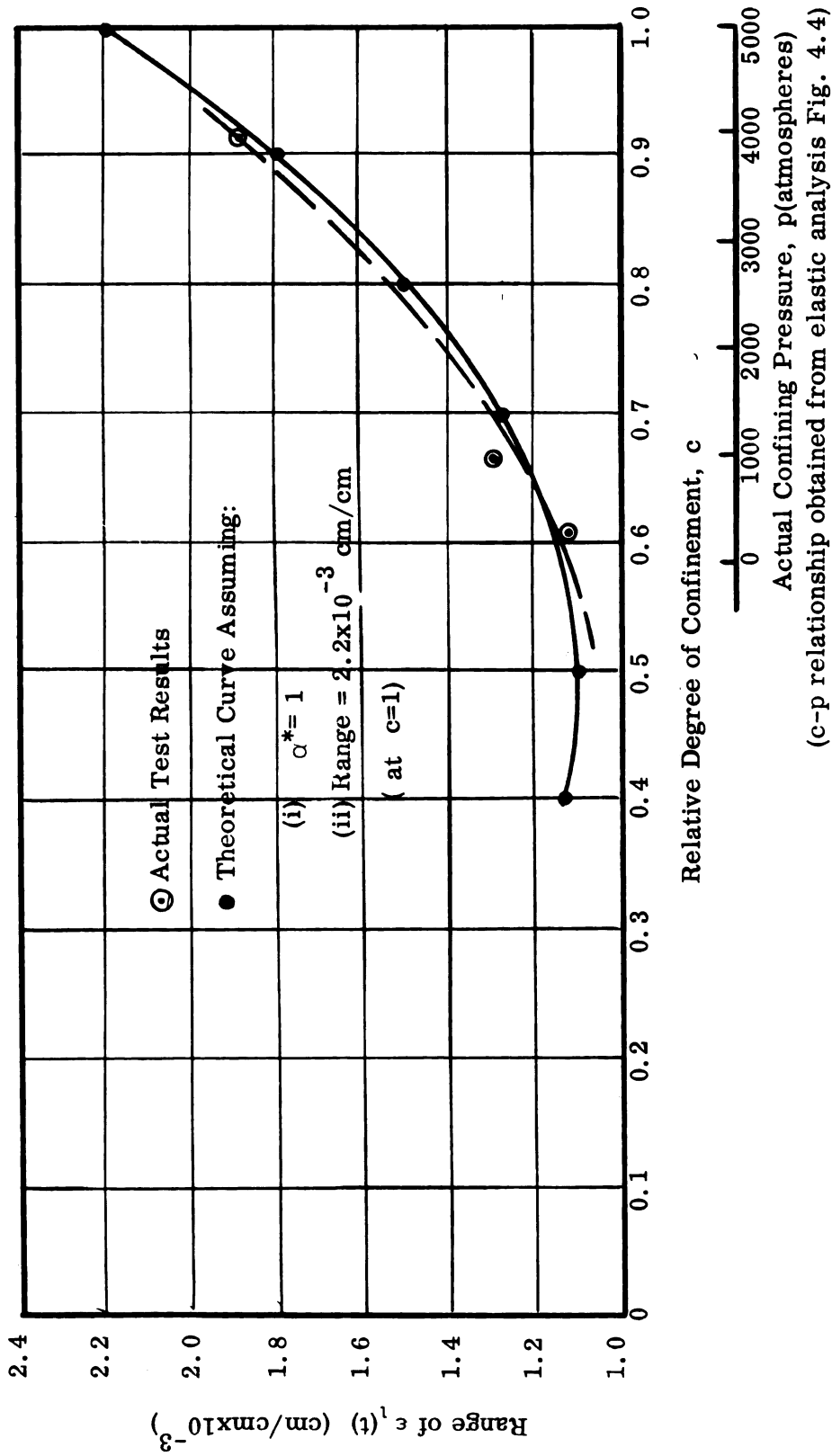


Fig. 4.9. Comparison of Theoretical and Actual Test Results for the Variation of the Range with Confining Pressure at Constant Differential Stress ($S=1500$ kg/cm²).

4.3 Variation of the Visco-Plastic Differential Strain Rate with Confining Pressure

From Robertson's creep curves (iv), (v) and (vi) in Fig. 4.6, it can be observed that they exhibit visco-plastic or steady state differential strain rates (their differential stress level being greater than or equal to the elastic limit) with the following values:

<u>Curve (iv)</u>	Confining Pressure = 2000 kg/cm ²
	Differential Stress = 5800 kg/cm ²
	Differential Strain Rate = 3.8×10^{-7} cm/cm/sec
<u>Curve (v)</u>	Confining Pressure = 3000 kg/cm ²
	Differential Stress = 4700 kg/cm ²
	Differential Strain Rate = 8.8×10^{-7} cm/cm/sec
<u>Curve (vi)</u>	Confining Pressure = 3000 kg/cm ²
	Differential Stress = 5700 kg/cm ²
	Differential Strain Rate = 12.5×10^{-7} cm/cm/sec

It is observed from curves (iv) and (vi) that with both curves being almost at the same differential stress level, an increase in the differential strain rate is observed merely as a result of the increase of the confining pressure. Also from curves (v) and (vi) which are at the same confining pressure of 3,000 kg/cm², an increase in the differential strain rate takes place again with increase in the differential stress level.

This variation is found to be qualitatively in good agreement with the theoretically expected variation; however, due to the undetermined values of the elements in the Bingham units of both systems, it is difficult to show

any fit between theoretical and actual values without at least knowing the approximate values of Y_2 and n_2 .

The actual values of the crystal grain system constants can be determined from the elastic analysis and from creep tests that should be conducted at a confining pressure corresponding to $c = 1$ and for different levels of constant differential stress.

CHAPTER V

SUMMARY AND CONCLUSIONS

5.1 Discussion

As a result of the interest that has developed at the beginning of this century, a study of the deformation of rocks under load was begun and several experiments were performed in an effort to establish the factors that affect the behavior of such materials.

One of the important factors that influences such a characteristic behavior, is the effect of confining pressure. Several empirical relationships incorporating this effect were presented. However, such relationships had serious shortcomings in describing accurately such a characteristic behavior, and have failed to account for the actual deformation mechanism that is responsible for such behavior.

The slow progress in this field of study is due to the following two reasons:

(i) It is a very expensive and tedious process to run experiments on rock at extremely high pressures, and to develop the necessary equipment by which such experiments can be performed.

(ii) The current theories of elasticity and viscoelasticity are inadequate to describe such characteristic behavior.

This inadequacy may be attributed in part to the fact that

rock is a heterogeneous material whose crystals possess physical properties which differ from the grain boundary properties.

In this investigation, the rock behavior is simulated by a rheological model composed of two independent systems, one representing the crystal properties and the second the properties of the grain boundaries. However, in order to be able to use this new model to describe the transitional behavior from uniaxial to triaxial stress state, it was necessary to redefine the effect of a general loading condition as a superimposed sum of a hydrostatic confining stress tensor and a differential stress tensor. As a result of this new formulation, three testing criteria for the usual case of a general principal compressive stress state were established in Chapter II, namely:

- (i) The uniaxial differential stress test
- (ii) The general biaxial differential stress test
- (iii) The balanced biaxial differential stress test

By utilizing this model, the separate contributions of the crystals and grain boundaries are correlated to the applied confining pressure by varying the position of the applied differential stress relative to the two systems according to the degree of confinement. This unique arrangement offers a basis for the mathematical analysis shown in Chapter III, where several variations in the characteristic behavior are displayed, depending on the ratio of the physical constants of one system to the other. The main characteristic

features that were obtained from the mathematical analysis can be summarized as follows:

- (i) In the elastic analysis, the equivalent elastic modulus increases with initial increase in confining pressure and decreases with subsequent increase in confining pressure depending on the value of α , which is the ratio of E_2 to E_1 .
- (ii) In the visco-elastic analysis, the creep range decreases with initial increase in the degree of confinement, c , and increases with subsequent increase of c depending on the value of α^* , which is the ratio of E_2^* to E_1^* . In addition, the initial slope of the visco-elastic creep curves either increases with increase in confining pressure or first decreases and then increases with subsequent increase in confining pressure, depending on the value of β^* which is the ratio of $1/\tau_2$ to $1/\tau_1$.
- (iii) In the visco-plastic analysis, the steady state creep rate first decreases and then increases with increase in the degree of confinement depending on the value of β , which is the ratio of η_2 to η_1 ; and it constantly increases with an increase in the differential stress.

This rheological description has been compared with existing data in Chapter IV yielding the following results:

- (a) by means of graphical fitting, it was possible to determine approximately the value of α , and the relationship between the degree of confinement, c , and the actual confining pressure, p . For the two particular cases that were presented, it was found that the relationship is linear, and that the minimum confining pressure needed to isolate the

effect of the crystals (corresponding to $c = 1$) is approximately 5,000 atmospheres.

(b) The range of the visco-elastic creep was found to increase with confining pressure, and from the variation obtained it was possible to approximately determine the value of α^* .

In this case, the initial slope of the visco-elastic response first decreased and then increased with increase in confining pressure.

(c) The steady state creep rate of the visco-plastic response was found to increase both with increase in confining pressure and differential stress; however, there was not enough data to obtain quantitative results.

Thus, with this rheological description of rock behavior it was possible to obtain results in excellent agreement with existing data and to provide a basis for understanding the variation of physical constants with changes in confining pressure.

5.2 Future Research

Based on this presentation, it was found that very few systematic tests were conducted on any particular kind of polycrystalline rock that would enable one to determine the ten physical constants of the model. This indicates the need for performing further experiments from which a complete analysis could be obtained.

In order to be able to fully determine the ten physical constants of the proposed model, the following experiments should be performed:

1. The first set of experiments is to obtain differential stress-strain curves of specimens which are subjected to various confining pressures. In this first type of experiments it is important to use an apparatus that is capable of furnishing the needed high pressure for determining the isolated physical property of the crystal grains. By analyzing the results of this first set of experiments, it will be possible to determine (i) the relationship between the degree of confinement c , and the actual confining pressure p ; and (ii) the approximate values of E_1 and E_2 .
2. The second set of experiments should be conducted to obtain, at various differential stress levels, creep data from specimens that are confined to a hydrostatic pressure which correlates to a degree of confinement of unity ($c=1$). From the results obtained it will be possible to determine E_2^* , η_2^* , η_2 and Y_2 .
3. The third set of experiments is conducted with the aim of obtaining, at a particular constant differential stress level, creep data from specimens that are subjected to various confining hydrostatic pressures. From the variation in the behavior due to the changes in confining pressures, it will be possible to roughly determine E_1^* , η_1^* , η_1 and Y_1 by fitting methods.

Other useful applications of this rheological representation are:

- (a) investigating the change in these physical constants with temperature by repeating the above three sets of experiments at various degrees of temperatures.

(b) studying the effect of temperature and pressure history on specimens by subjecting them in the laboratory to various predetermined history conditions.

(c) determining the value of Poissons ratio of each system from the elastic analysis of differential stress-strain curves by performing first a set of uniaxial differential stress tests at various constant confining pressures followed by a set of balanced biaxial differential stress tests at the same constant confining pressures.

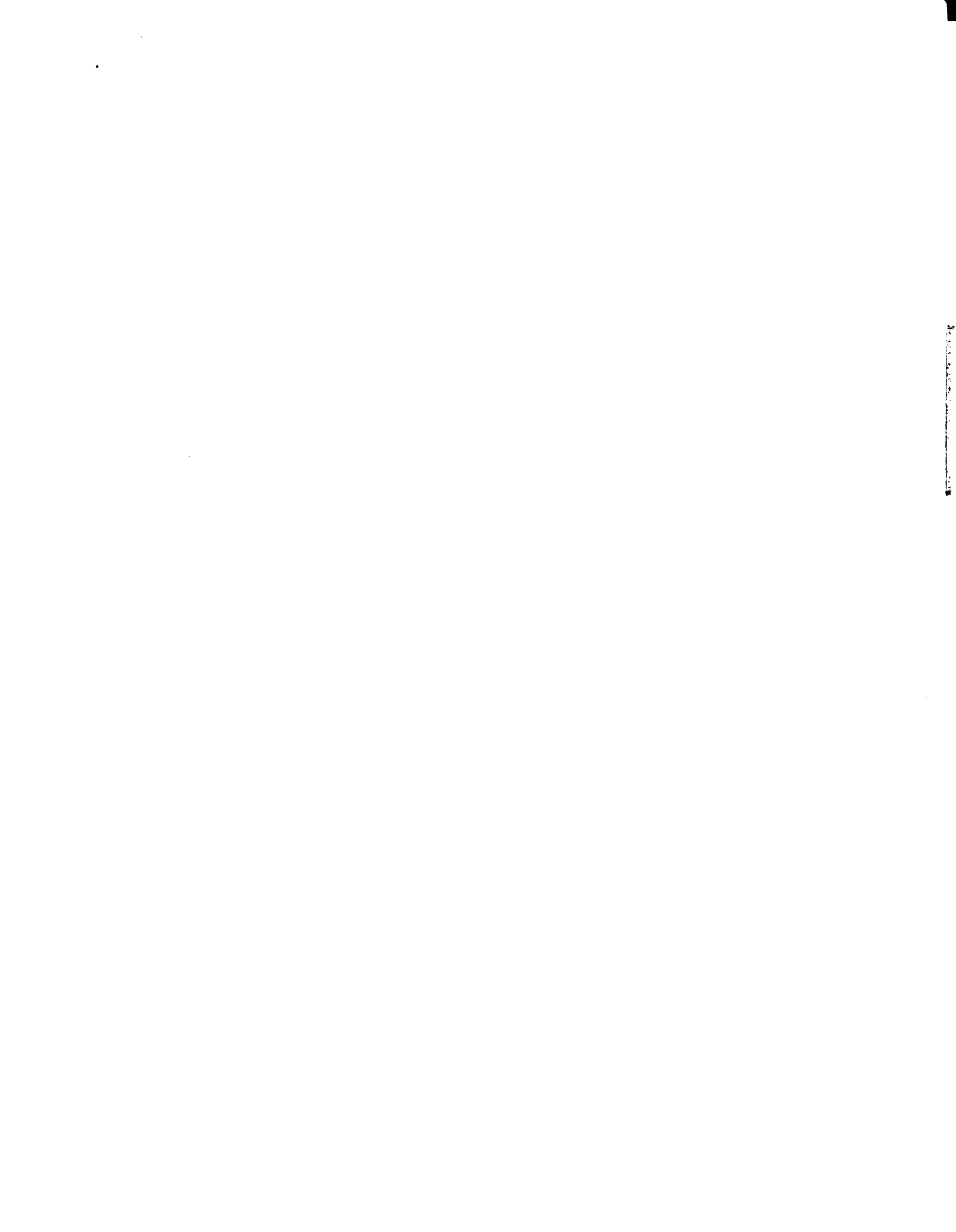
(d) although this analysis is only valid for single phase polycrystalline materials, yet it may serve as a first step towards analyzing more complicated mechanisms of deformation that are exhibited in the behavior of multi-phase polycrystalline materials such as ice.

BIBLIOGRAPHY

1. Adams, F. D., and Nicholson, J. T., "An Experimental Investigation into the Flow of Marble," Proc. Roy. Soc. London, Ser. V., Vol. 195, 1901, pp. 363-401.
2. _____. "An Experimental Investigation into the Action of Differential Pressure on Certain Minerals and Rocks, Employing the Process Suggested by Prof. Kick," Jour. Geol., Vol. 18, 1910, pp. 485-525.
3. _____. "An Experimental Contribution to the Question of the Depth of the Zone of Flow in the Earth's Crust," Jour. Geol., Vol. 20, 1912, pp. 97-118.
4. _____. and Bancroft, J. A., "On the Amount of Internal Friction Developed in Rocks During Deformation and on the Relative Plasticity of Different Types of Rocks," Jour. Geol., Vol. 25, pp. 597-637.
5. Baron, G., Habib, P., and Morlier, P., "Deformation of Rocks under Constraint," Review de l'institute Francais du Petrole, June 1963, pp. 97-130. (in French)
6. Bland, D. R., The Theory of Linear Visco-elasticity, New York, Pergamon Press, 1960, pp. 125.
7. Böker, R., "Die Mechanik der bleibenden Formänderungen in Kristallinisch aufgebauten Körpern," Verdeutsch, Ingenieure Mitt. Forschungsarbeiten, Vol. 175, 1915, pp. 1-51.
8. Brace, W. F., "Brittle Fracture of Rocks," International Conference on State of Stress in Earth Crust, May 1963.
9. Cottrell, A. H., "Dislocation and Plastic Flow in Crystals," Oxford, Clarendon Press, 1952.
10. Cullity, B. D., "Elements of X-Ray Diffraction," Addison Wesley Publishing Company, 1956.
11. Eirich, F. R., editor, Rheology, theory and applications, Vol. 1, New York, Academic Press, Inc., 1956.
12. Emery, C. L., "Strain Energy in Rocks," International Conference on State of Stress in Earth Crust, May 1963.
13. _____. "Testing Rock in Compression," Mine and Quarry Engineering, April and May, 1960.

14. Finnie, I., and Heller, W. R., Creep Engineering Materials, McGraw-Hill Book Company, Inc., New York, 1959.
15. Griggs, D. T., "Deformation of Rocks under High Confining Pressure," J. Geology, Vol. 44, 1936, pp. 541-577.
16. _____. "Creep of Rocks," J. Geology, Vol. 47, 1938, p. 225.
17. _____. "Experimental Flow of Rocks under Conditions Favoring Re-crystallization," Bulletin of Geological Society of America, Vol. 51, July 1940, pp. 1001-1022.
18. Handin, J., "An Application of High Pressure in Geophysics," Trans. A.S.M.E., Vol. 75, 1953, pp. 315-324.
19. _____. and Hager, R. V., "Experimental Deformation of Sedimentary Rocks under Confining Pressure," Am. Assoc. Petrol. Geol. Bulletin, Vol. 41, 1957, pp. 1-50.
20. Heard, H. C., "Transition from Brittle Fracture to Ductile Flow in Solenhofen limestone as Function of Temperature, Confining Pressure, and Interstitial Fluid Pressure," Geol. Soc. Am. Memoirs, Vol. 79, pp. 193-226, 1960.
21. Hill, R., "Mathematical Theory of Plasticity," Oxford, Clarendon Press, 1956.
22. Kê, T. S., "Experimental Evidence of the Viscous Behavior of Grain Boundaries in Metals," Physics Review, Vol. 71, No. 8, 1947, pp. 533-546.
23. Kvapil, R., "Tectonic Experiments on Natural Rocks," Int. Jour. of Rock Mech. and Mining Sciences, Vol. 1, Jan., 1964.
24. Murrell, S. A. F., and Misra, A. K., "Time-dependent Strain or 'Creep' in rocks and Similar non-metallic Materials," Inst. Mining Metall. Bull., Vol. 71, pt. 7., 1962, pp. 353-378.
25. Nadai, A., Theory of Flow and Fracture of Solids., Vol. 1, McGraw-Hill Book Co., New York, 1950, pp. 175-228.
26. Price, N. J., "A Study of Time-Strain Behavior of Coal-Measure Rocks," International of Rock Mechanics and Mining Sciences, Vol. 1, No. 2, March 1964.
27. Read, W. T., Dislocations in Crystals, New York, McGraw-Hill Book Co., Inc., 1953.

28. Robertson, E. C., "Experimental Study of the Strength of Rocks," Bull. Geol. Soc. of America, Vol. 66, Oct. 1955, pp. 1275-1314.
29. _____. "Visco-elasticity of Rocks," International Conference on State of Stress in the Earth's Crust, May 1963.
30. _____. "Creep of Solenhofen Limestone under Moderate Hydrostatic Pressure," Geol. Soc. Amer. Memoir, Vol. 79, 1960, pp. 227-244.
31. Schwartz, A. E., "Failure of Rock in Triaxial Shear Test," Proceedings of the Sixth Symposium on Rock Mechanics, 1964.
32. Seligman, G., "The growth of glacier crystals," Journal of Glaciology, pp. 254, 1949.
33. Steineman, S., "Flow and Recrystallization of ice," Association Internationale d'Hydrologie Scientifique, Publication no. 39, Congres de Rome, 1954.
34. Tomashevskaya, I. S., "A Study of Shear Modulus of Rocks under High Confining Pressure," Izv. Akad. Nauk, Vol. 18, Geophysics Series, 1961, (in Russian).
35. Von Karman, T., "Festigkeitsversuche unter allseitigem Druck," Zeitschr. Ver. deutsch. Ingenieure, Vol. 55, 1911, pp. 1749-1757, (in German).
36. Zener, C., Elasticity and anelasticity of metals, Chicago, University of Chicago Press, 1948, pp. 140-163.



MICHIGAN STATE UNIVERSITY LIBRARIES



3 1293 03174 7532